Binding of a glaucoma-associated myocilin variant to the αB-crystallin chaperone impedes protein clearance in trabecular meshwork cells

Received for publication, June 5, 2018, and in revised form, October 19, 2018 Published, Papers in Press, November 2, 2018, DOI 10.1074/jbc.RA118.004325

Jeffrey M. Lynch[‡1], Bing Li[‡], Parvaneh Katoli[‡], Chuanxi Xiang[‡], Barrett Leehy[‡], Nalini Rangaswamy[‡], Veronica Saenz-Vash[§], Y. Karen Wang[§], Hong Lei[¶], Thomas B. Nicholson[‖], Erik Meredith[**], Dennis S. Rice[‡], Ganesh Prasanna[‡], and Amy Chen[‡]

From [‡]Ophthalmology, [§]Analytical Sciences and Imaging, [¶]Laboratory Animal Services, [‖]Chemical Biology and Therapeutics, and [**]Global Developmental Chemistry, Novartis Institutes for BioMedical Research, Cambridge, Massachusetts 02139

Edited by Paul E. Fraser

Myocilin (*MYOC*) was discovered more than 20 years ago and is the gene whose mutations are most commonly observed in individuals with glaucoma. Despite extensive research efforts, the function of WT MYOC has remained elusive, and how mutant MYOC is linked to glaucoma is unclear. Mutant MYOC is believed to be misfolded within the endoplasmic reticulum, and under normal physiological conditions misfolded MYOC should be retro-translocated to the cytoplasm for degradation. To better understand mutant MYOC pathology, we CRISPR-engineered a rat to have a MYOC Y435H substitution that is the equivalent of the pathological human MYOC Y437H mutation. Using this engineered animal model, we discovered that the chaperone αB-crystallin (CRYAB) is a MYOC-binding partner and that co-expression of these two proteins increases protein aggregates. Our results suggest that the misfolded mutant MYOC aggregates with cytoplasmic CRYAB and thereby compromises protein clearance mechanisms in trabecular meshwork cells, and this process represents the primary mode of mutant MYOC pathology. We propose a model by which mutant MYOC causes glaucoma, and we propose that therapeutic treatment of patients having a *MYOC* mutation may focus on disrupting the MYOC–CRYAB complexes.

Primary open-angle glaucoma (POAG)[2] is a multifactorial, chronic condition, and people with glaucoma generally experience a gradual loss of peripheral vision, which is due to the death of retinal ganglion cells (RGCs). The risk of glaucoma increases with age, and glaucoma is a major cause of blindness worldwide with the global patient population in 2020 estimated to be 80 million people (1). In the United States, more than 80% of the people with glaucoma have POAG (2) and most exhibit elevated (>21 mm Hg) intraocular pressure (IOP). High IOP is a risk factor for POAG as the optic nerve is very sensitive and can be damaged by high pressure (3).

Steroid-induced glaucoma constitutes a major subset of glaucoma patients. The first gene with mutations associated with glaucoma was identified at the GLC1A locus on chromosome 1q21-q31 (4, 5) and was called trabecular meshwork-inducible glucocorticoid response (*TIGR*) because its expression is up-regulated following dexamethasone treatment. The *TIGR* gene was later renamed to myocilin (*MYOC*) due to shared identity with myosin (6). At present, *MYOC* mutations remain the most common gene mutation found in glaucoma patients (7). *MYOC* mutations are found in 2–4% of all POAG patients (8, 9) and over one-third of all patients (10) with juvenile open-angle glaucoma (JOAG). Uniquely, it has been reported that only people that are heterozygous for a *MYOC* mutation develop glaucoma, although those homozygous do not (11). The most common *MYOC* mutation introduces an early stop codon, Q368X, and it is reported in over one-third of glaucoma patients carrying a *MYOC* mutation (12). To date, there are >70 pathological *MYOC* mutations reported (www.myocilin.com)[3] (92), and most of these mutations are found in exon 3, which encodes for the C terminus of MYOC. Interestingly, an *in vitro* observation is that N-terminal pathological MYOC mutants are secreted, although the C-terminal pathological MYOC mutant proteins are not secreted (13, 14).

Patients with a *MYOC* mutation are estimated to be 25% younger than the general POAG population (15), and these patients typically exhibit extremely high IOPs (16) that may not be adequately lowered by current IOP-lowering medica-

This work was supported by Novartis Institutes for BioMedical Research. Authors are all employees of Novartis Institutes for BioMedical Research (NIBR) and receive salary. As NIBR is a publicly traded pharmaceutical company, the authors may hold stock.

This article contains Figs. S1–S5.

[1] To whom correspondence should be addressed: Ophthalmology, Novartis Institutes for BioMedical Research, 22 Windsor St., Cambridge, MA 02139. Tel.: 617-871-3422; E-mail: jeffrey.lynch@novartis.com.

[2] The abbreviations used are: POAG, primary open-angle glaucoma; AH, aqueous humor; TM, trabecular meshwork; BAC, bacterial artificial chromosome; ThT, thioflavin T; ER, endoplasmic reticulum; ERAD, ER-associated degradation; IOP, intraocular pressure; NFL, nerve fiber layer; RPE, retinal pigment epithelium; Ub, ubiquitin; GAPDH, glyceraldehyde-3-phosphate dehydrogenase; IHC, immunohistochemistry; RGC, retinal ganglion cell; JOAG, juvenile open-angle glaucoma; DMEM, Dulbecco's modified Eagle's medium; FBS, fetal bovine serum; HMW, high-molecular weight; PTS, peroxisomal targeting signal; α-SMA, α-smooth muscle actin; COLIV, collagen IV; CMV, cytomegalovirus; OCT, optical coherence tomography; IP, immunoprecipitation; ERG, electroretinography; AP, alkaline phosphatase; STR, scotopic threshold response; PDI, protein-disulfide isomerase.

[3] Please note that the JBC is not responsible for the long-term archiving and maintenance of this site or any other third party hosted site.

tions (17, 18). Penetrance of the *MYOC* mutant gene in families reported to have a history of glaucoma has been suggested to be as high as 90% (19); however, a more recent study suggests that penetrance of a *MYOC* mutation in the general population is likely much lower (20). Nevertheless, there remains a large glaucoma patient population with a *MYOC* mutation, and these patients have a medical need that is not sufficiently met.

In mice, Northern blots have suggested that MYOC has a limited tissue distribution, with transcripts found in eye, skeletal muscle, and heart (21–23). *Myoc*-deficient mice have been created, and these null animals have normal trabecular meshwork (TM) histology and normal IOP, and they do not develop glaucoma (24). Numerous researchers have attempted to gain understanding of mutant MYOC by creating various MYOC transgenic mice (25–27). In all these early transgenic models, no animals showed a statistically-significant IOP elevation. It was later hypothesized that the reason for this lack of a glaucoma phenotype in rodents is because human MYOC has a cryptic C-terminal (−SKM) peroxisomal targeting signal (PTS) that is not conserved in MYOC from other species (28). Support for the PTS theory came from mice that exhibited IOP elevation following ocular injection of CMV-driven human MYOC adenoviruses (28). Although the SKM sequence is essential for weak binding to peroxisomal targeting signal type 1 receptor (PTSR1), the sequence is not sufficient for peroxisomal import because of the fact that the PTS1 is much longer and is believed to be a dodecamer (29–31). Within the PTS1 dodecamer, optimal residues from the tripeptide have been identified at −2 and −5 (32), and these hydrophobic residues are not found in human MYOC. Since publication of the MYOC–PTS hypothesis, the C-terminal structure of human MYOC has been solved, and the SKM signal of MYOC has been found not to be cryptic (33), thus suggesting that there may be an alternative explanation for the IOP phenotype observed following CMV–MYOC adenovirus injection. More recently, a CMV-driven human MYOC Y437H mutant transgenic mouse line was created and reported to have IOP elevation with notable RGC loss (34). In this CMV–MYOC–Y437H model, the authors attributed pathology associated with mutant MYOC to endoplasmic reticulum (ER) stress (34). CMV is a very robust promoter with potential to cause protein overexpression that exceeds any normal or diseased physiological protein expression range. As MYOC is a secreted protein processed in the ER, CMV driving its overexpression should be anticipated to challenge the protein-processing capacity of any cell resulting in up-regulation of ER and ER-associated proteins. Hence, a limitation of robust CMV-driven animal models could be artifacts arising from pronounced overexpression.

The purpose of our work was to enhance biological understanding of mutant MYOC, so we utilized CRISPR technology to engineer a rat to have a pathological MYOC Y435H mutation. The rat MYOC Y435H mutation corresponds to the severe human MYOC Y437H mutation associated with JOAG (8, 35). By studying mutant MYOC in an *in vivo* model where expression is physiologically relevant, we were able to discover a novel protein–protein interaction between MYOC and CRYAB. *In vitro* experiments substantiated the interactions as we found that mutant MYOC can aggregate with CRYAB. Furthermore, to validate findings from our MYOC Y435H rat model, we generated two bacterial artificial chromosome (BAC) transgenic mouse lines, one with expression of human WT MYOC, and the other with the most common pathological human MYOC mutation, Q368X. By discovering the MYOC–CRYAB interaction, our findings provide new insight into how mutant MYOC causes pathology. We propose that targeting/disrupting the MYOC–CRYAB complex is a therapeutic strategy to maintain proper cell function and ultimately help the glaucoma patient with a *MYOC* mutation retain their vision and avoid blindness.

Results

As *MYOC* gene mutations are the most common mutation detected in glaucoma patients, there is substantial interest in understanding the role of MYOC in the eye. By Western blot analysis, human MYOC protein migrates under denaturing conditions slightly greater than 50 kDa and appears as a doublet due to partial *N*-glycosylation (36). The basal level of MYOC in human aqueous humor (AH) is low, but it is detectable by Western blotting (Fig. 1*A*). The *MYOC* gene has been reported to be stress-induced (37) and is reported to be higher in glaucomatous eyes compared with nondiseased eyes (14). By Western blotting, we observed increased MYOC protein in AH collected from cadaver eyes (Fig. 1, *A* and *B*) compared with the level observed in AH from living donors. The increased MYOC in cadaver eyes could be due to hypoxia stress and/or due to some cell lysis occurring following death, and this may obscure what would be a higher MYOC level anticipated in glaucoma patient samples. Immunohistochemical (IHC) analyses showed that in human eyes MYOC has the greatest expression throughout the TM tissue (Fig. 1*C*) with lesser amounts observed in the ciliary body and retina (Fig. S1).

CRISPR-engineered MYOC mutant rat

Our CRISPR-engineered MYOC Y435H rat was developed (Fig. 2*A*) and created by Horizon Labs (St. Louis, MO). Off-target effects of CRISPR are rare, and quality control to ensure integrity of the *Myoc* gene was completed by Horizon Labs. Sequencing of PCR products (Genewiz, Cambridge, MA) from rat genomic DNA confirmed that the rat model had been successfully generated (Fig. 2*B*). Western blot analysis of rat eye limbal ring extracts indicated a band at the expected protein size for monomeric MYOC (Fig. 2*C*). Rodent MYOC lacks the glycosylation site found in human MYOC, so no doublet is observed in the Western blottings. The Western blottings do show that expression of soluble MYOC in heterozygote and homozygote CRISPR-engineered rats was similar to that for the WT rats (Fig. 2, *C* and *D*); hence, our CRISPR-engineered rat model was expressing MYOC protein within a normal physiological range.

IOP for aged cohorts of WT, heterozygous, and homozygous MYOC Y435H rats was monitored for several months (Fig. 3*A*). IOP was found not to differ among the animal cohorts based on time of day (Fig. S2). MYOC expression is known to be up-regulated by steroid treatment (38, 39), and some rat cohorts were treated with prednisolone and their IOP monitored during the

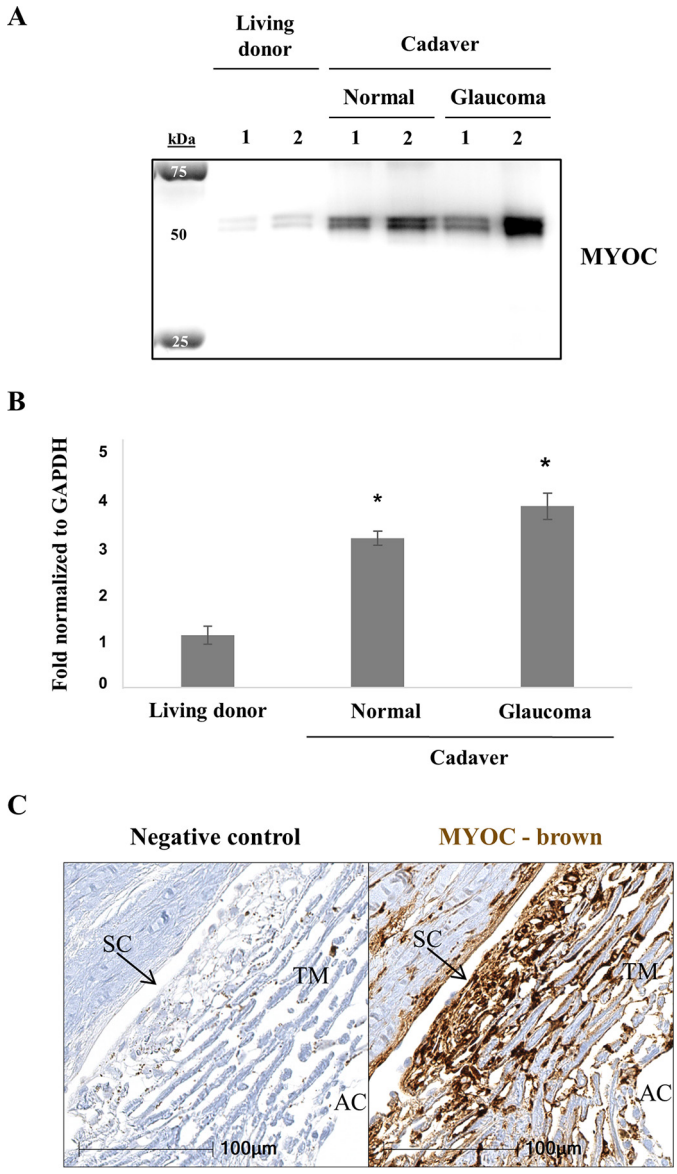

Figure 1. MYOC protein is found in human AH, and in the eye tissue, the highest MYOC expression is observed in the trabecular meshwork. *A,* Western blotting for MYOC protein in human AH collected from different living donor eyes as well as from different deceased donor eyes. All AH samples were from donors of a similar elderly age, and no donors had a *MYOC* mutation. For the Western blotting, 5 μg of each sample was loaded per well, and anti-MYOC antibody is from R&D Systems. *B,* human AH sample Western blots were quantified. *Error bars* are $\pm$ S.D., and * indicates *t* test $p < 0.05$. *C,* control immunohistochemistry image of the human TM region and an image stained to show MYOC expression (MYOC indicated by the *brown color*) in the TM region. High expression of MYOC is evident in the TM. MYOC expression was observed in other regions of the eye (Fig. S1), but at a lower expression than that observed for the TM. Abbreviations used are as follows: *AC*, anterior chamber; *SC*, Schlemm's canal.

2 months of treatment. Prednisolone treatment resulted in an increase in IOP for all three groups of animals; however, IOP for heterozygote and homozygote animals did not differ significantly from that of the WT rats (Fig. 3*A*). Additionally, when we examined the TM of the animals by H&E, trichrome, and immunohistochemical methods, we did not observe any major differences in outflow pathway morphology nor changes in cytoskeletal and extracellular matrix among the three groups either before (Fig. 3*B*) or after steroid treatment (Fig. 3*B*). Similar results for IOP and TM histology were observed for another two aged rat cohorts.

Our cumulative findings, including those from Western blot analysis, had suggested that MYOC Y435H heterozygote and homozygote rats are very similar to each other and both had some minor differences when compared with WT rats. As the published literature focuses on human MYOC heterozygote phenotypes, we limited our rat RGC analysis to a comparison of WT and heterozygotes. When retinal structure and function were evaluated in 18-month-old WT and heterozygote rats, no significant differences in retinal thickness (assessed by optical coherence tomography (OCT)) and function, specifically a- and b-wave (assessed by electroretinography (ERG)) were observed between mutant MYOC Y435H heterozygous and WT MYOC animals (Fig. 4).

Dark-adapted ERGs were recorded from mutant MYOC Y435H heterozygous and WT MYOC rats at 18 months of age. In rats, the positive and negative scotopic threshold responses (STR) are primarily generated by ganglion cells with minimal amacrine cell contribution (40). These responses were assessed using low-intensity stimuli at -6.0, -5.5, and -5.0 log cd·s/m^2. No significant differences in pSTR and nSTR amplitudes were observed between MYOC Y435H heterozygous and WT MYOC rats (Fig. 4*A*) suggesting normal ganglion cell function associated with MYOC Y435H heterozygosity. Photoreceptor function was assessed with a high-intensity 2.2 log cd·s/m^2 stimulus (Fig. 4*B*). At high-stimulus intensity the photoreceptor response (a-wave) is primarily rod-dominated with a smaller contribution generated from cone cells (41). No significant differences in photoreceptor function and on-bipolar cell function (b-wave) were observed between groups (Fig. 4*B*). At 18 months of age, OCT images of the retina were acquired using a spectral domain OCT system. Two b-scans were manually centered on the optic nerve head and acquired in the vertical and horizontal orientations from each eye and assessed for morphological abnormalities (Fig. 4*C*). Cell loss was assessed by quantifying retinal thickness between the nerve fiber layer (NFL) and the RPE. OCT scans did not reveal any morphological abnormalities nor cell loss in the mutant MYOC Y435H heterozygous rats (Fig. 4*C*). These results suggest that the presence of mutant MYOC did not adversely impact retina development nor did mutant MYOC cause a loss of RGCs or adversely impact retina function.

MYOC Q368X BAC mice

Findings for mouse mutant *Myoc* Y423H BAC mice (25) and human mutant *MYOC* Y437H BAC mice (26, 42) have previously been reported, and the animals exhibited low to no IOP increase. Similarly, we observed no IOP differences between 6- and 8-month-old WT mice and MYOC Q368X BAC mice (Fig. S3) and no morphological abnormalities in the eye. This animal model was utilized to validate findings made in the CRISPR-engineered MYOC Y435H rat model (Fig. S4).

CRYAB identified as a MYOC-binding partner

Several studies have been conducted to identify protein-binding partners for MYOC in the hope of defining a putative function for this protein (43–45). To identify proteins of inter-

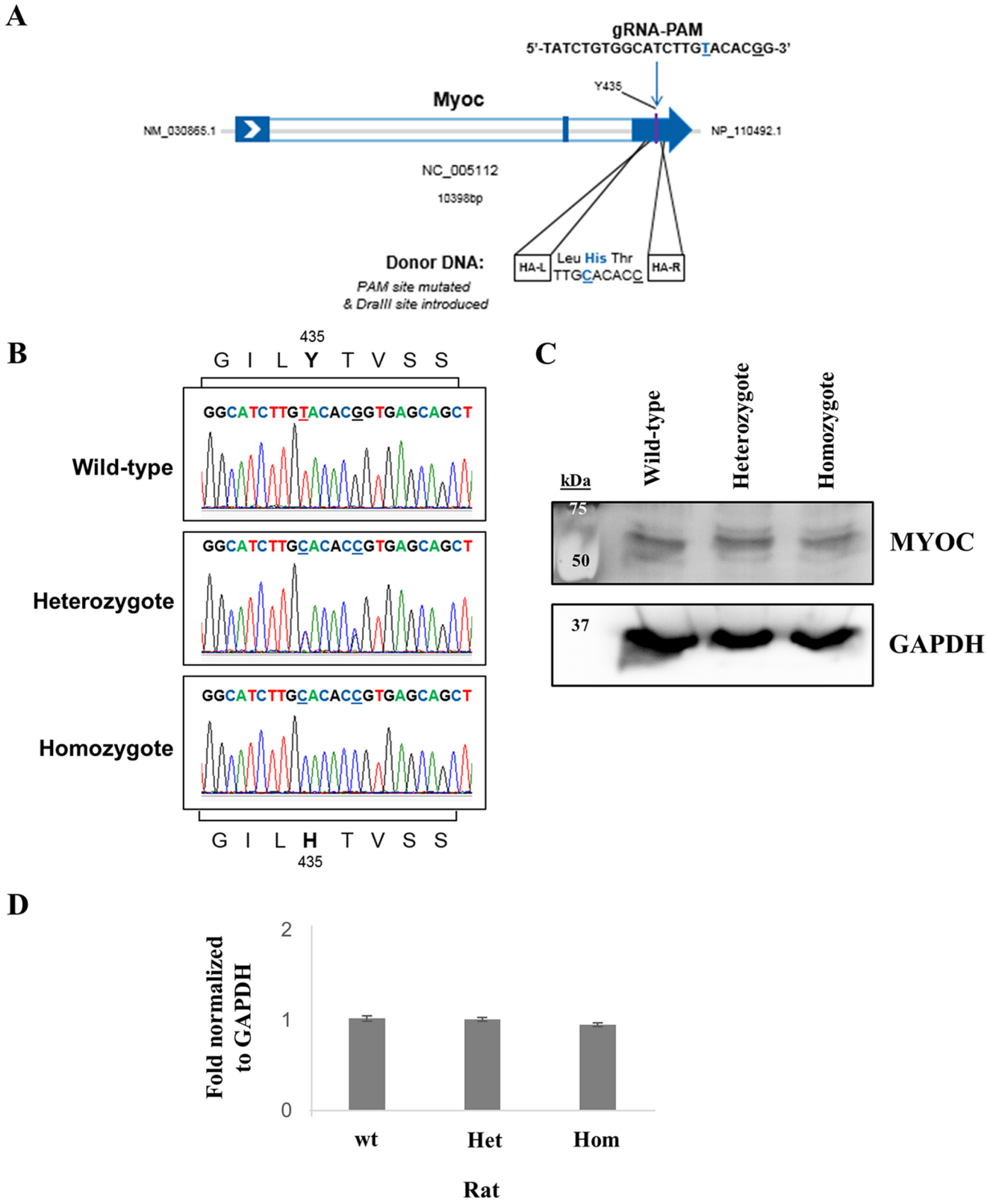

Figure 2. Generation and confirmation of rats with the Myoc Y435H mutation. *A,* CRISPR/Cas9–based strategy to introduce Y435H point mutation in rat *Myoc*. *B,* sequencing traces of Myoc PCR products amplified from rat genomic DNA isolated from tail biopsies. Sequencing results confirm both the Y435H point mutation and the silent (PAM site) mutation in the heterozygote and homozygote animals (sites of mutation are *underlined*). *C,* Western blotting of soluble Myoc in rat limbal ring lysates (40 μg of samples) using anti-MYOC antibody from Acris. *D,* rat limbal ring lysate Western blots were quantified. *Error bars* are ± S.D., and *t* tests showed $p > 0.1$. Abbreviations used are as follows: *HA-L,* left homology arm; *HA-R,* right homology arm; *Het,* heterozygote; *Hom,* homozygote; *wt,* WT.

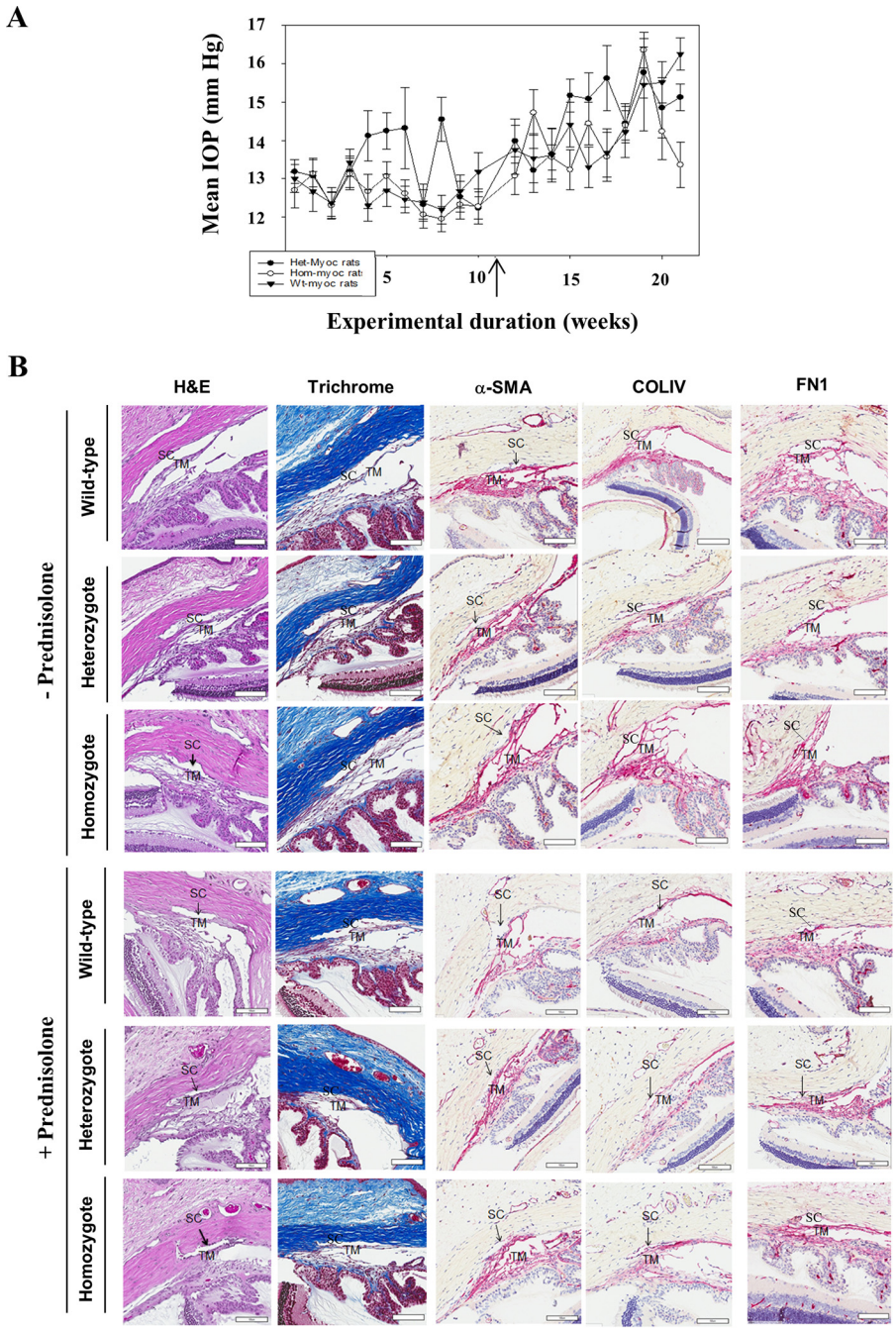

Figure 3. Rats with the Myoc Y435H mutation have IOP and TM histology (at 9 months of age) that does not differ from WT rats, and this did not change following prednisolone challenge. *A,* IOP was monitored in a 4-month-old cohort of 10 WT (*wt*), 10 heterozygote (*Het*), and 10 homozygote (*Hom*) rats before and after implantation of a prednisolone pellet (25 mg for 60 days). *Arrow* indicates time of implantation. Results are ± S.E. *B, top,* H&E and trichrome staining of TM of 9-month-old rats that were not treated with prednisolone. Immunohistochemical images for α-SMA, COLIV, and FN1 (*red color*) indicated that the WT rats did not have tissue expression of these proteins that differed from the rats with a Myoc Y435H mutation. *Bottom,* H&E and trichrome staining of 9-month-old rat eyes from animals treated with prednisolone. Immunohistochemical images for α-SMA, COLIV, and FN1 for 9-month-old rats that received prednisolone treatment. Abbreviation used is as follows: *SC*, Schlemm's canal. *Scale bars* are 100 μm.

est potentially associated with MYOC, we completed small-scale proteomic analysis of rat AH. Mass spectrometry (MS) analysis of AH samples collected from heterozygote rats provided evidence that animals with mutant MYOC harbored differences in protein composition from WT animals. MS analysis revealed that the AH from WT animals had higher expression of many crystallin proteins (*e.g.* CRYAA, CRYAB, CRYBA2, and CRYBB3) compared with animals with mutant MYOC Y435H (Table 1). Next Generation Sequencing data from primary human TM cell lines[4] identified CRYAB as the highest expressed crystallin family member in the TM. Western blot analysis of rat AH samples supported the MS data as WT animals were found to have more soluble CRYAB than animals with a MYOC Y435H mutation (Fig. 5, *A–D*). Additionally, immunocytochemistry staining of TM tissues from 18-month-old WT

[4] A. Chen, unpublished data.

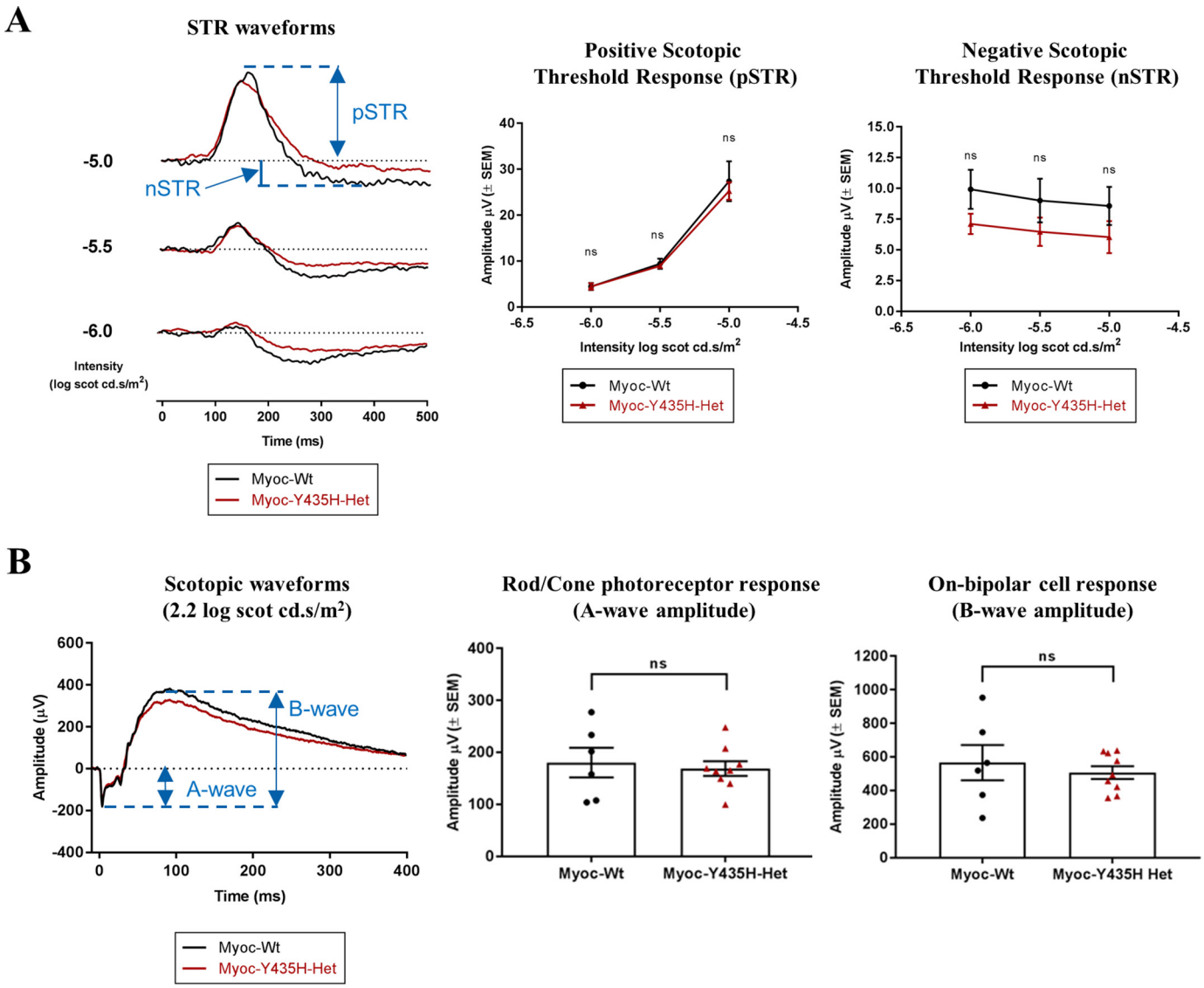
A
STR waveforms
pSTR
nSTR
-5.0
-5.5
-6.0
Intensity (log scot cd.s/m²)
0 100 200 300 400 500
Time (ms)
Myoc-Wt
Myoc-Y435H-Het
Positive Scotopic Threshold Response (pSTR)
Amplitude µV (± SEM)
ns
Intensity log scot cd.s/m²
Myoc-Wt
Myoc-Y435H-Het
Negative Scotopic Threshold Response (nSTR)
Amplitude µV (± SEM)
ns
Intensity log scot cd.s/m²
Myoc-Wt
Myoc-Y435H-Het
B
Scotopic waveforms (2.2 log scot cd.s/m²)
Amplitude (µV)
B-wave
A-wave
Time (ms)
Myoc-Wt
Myoc-Y435H-Het
Rod/Cone photoreceptor response (A-wave amplitude)
Amplitude µV (± SEM)
ns
Myoc-Wt
Myoc-Y435H-Het
On-bipolar cell response (B-wave amplitude)
Amplitude µV (± SEM)
ns
Myoc-Wt
Myoc-Y435H Het
C
MYOC-wt
MYOC-Y435H-Het
Total retinal thickness (NFL →RPE)
Thickness µm (±SEM)
ns
Myoc-Wt
Myoc-Y435H-Het

Table 1
Summary table highlighting proteins detected by LC-MS analysis to be in pooled aqueous humor samples collected from WT rats and from rats heterozygous for mutant MYOC Y435H ($n = 10$ animals per group)
Peak area is area under curve (AUC).

Protein name	Gene	Accession no.	Mass	No. of unique peptides	Wildtype	Heterozygote
			kDa		*AUC*	*AUC*
α-Crystallin-A	*Cryaa*	P24623	22.4	23	1.60E + 11	9.50E + 08
α-Crystallin-B	*Cryab*	P23928	20.0	15	5.50E + 10	3.40E + 08
β-Crystallin-A2	*Cryba2*	Q8CGQ0	22.2	9	1.90E + 10	2.80E + 07
β-Crystallin-A3	*Cryba1*	P14881	25.3	17	1.60E + 10	7.60E + 07
β-Crystallin-A4	*Cryba4*	P56374	22.4	14	6.80E + 09	1.30E + 08
β-Crystallin-B1	*Crybb1*	P02523	28.1	21	2.60E + 10	5.30E + 07
β-Crystallin-B2	*Crybb2*	P62697	23.4	27	1.20E + 11	2.90E + 08
β-Crystallin-B3	*Crybb3*	P02524	24.3	20	1.90E10	2.30E + 07
Cathepsin D	*Ctsd*	P24268	44.7	7	2.90E + 07	4.60E + 07
Complement C3	*C3*	P01026	186.5	99	4.00E + 09	2.70E + 09
Complement C4	*C4*	P08649	192.2	10	9.40E + 07	8.30E + 07
Serotransferrin	*Tf*	P12346	76.4	57	3.50E + 10	1.50E + 10
Serum albumin	*Alb*	P02770	68.7	5	4.10E + 10	2.90E + 10

and mutant MYOC Y435H rats showed more intensive staining of CRYAB in the WT animal (Fig. 5*E*). An immunoprecipitation (IP) experiment revealed that CRYAB bound WT MYOC (Fig. 5*F*). Supporting evidence of a MYOC–CRYAB interaction was observed via an additional IP experiment that was completed using a cell line (G401) that has endogenous expression of both MYOC and CRYAB (Fig. S5). Findings from these IP experiments are important as protein binders to MYOC are poorly defined and tentatively identified binders have lacked validation.

It has been suggested that mutant MYOC accumulates in the ER and causes pathology because of ER stress (34, 46–48). When we examined whole-eye extracts from 18-month-old animals by Western blotting, we observed no up-regulation of proteins indicative of ER stress (*i.e.* BiP, CALR, PDI, and GRP94), which is in agreement with that previously reported for another mutant MYOC animal model (49). However, what we did observe by Western blotting was an accumulation of high-molecular weight (HMW) ubiquitinated (Ub) proteins (Fig. 6, *A* and *B*). This accumulation of HMW ubiquitinated proteins in the rats with the MYOC Y435H mutation suggests that the proteasome and protein clearance mechanisms are not working effectively. To see whether protein clearance was compromised in another mutant MYOC animal model, we examined two MYOC BAC mouse lines. One line is a BAC transgenic with WT human MYOC, whereas the second line is a BAC transgenic with a Q368X point mutation in human MYOC. MYOC was identified in whole-eye extracts using R&D Systems anti-MYOC antibody, which is an antibody that strongly reacts with human MYOC and has weak cross-reaction with mouse MYOC (Fig. S4*A*). Western blot analysis of whole-eye extracts from 6- to 8-month-old BAC mice did not show any indication of ER stress. However, the WT MYOC BAC transgenics had a modest increase in soluble CRYAB; in comparison, the mutant MYOC Q368X BAC had less soluble CRYAB and more HMW ubiquitinated proteins (Fig. S4, *A* and *B*). These findings from BAC mice were in agreement with our MYOC Y435H rat model. Therefore, we have myocilin *in vivo* models that do not show ER stress, but 1) suggest a correlation exists between MYOC and CRYAB; 2) indicate there is an accumulation of HMW ubiquitinated proteins when mutant myocilin is present; and 3) support a hypothesis that mutant myocilin is forming insoluble complexes with CRYAB, which has the potential to compromise protein degradation pathways.

Presence of CRYAB causes an increase in insoluble mutant MYOC

To further test our hypothesis that mutant MYOC forms insoluble complexes with CRYAB, we transiently-transfected NTM5 cells with different MYOC cDNAs ± CRYAB. From our Next Generation Sequencing data[3] for human TM cells as well as from previous Western blottings, we knew that NTM5 cells do not express MYOC or αB-CRYAB proteins. As others have reported, WT MYOC is efficiently secreted *in vitro,* although pathological mutant MYOCs are not (13, 14). Western blot analysis comparing soluble and insoluble fractions from transfected NTM5 cells indicated that presence of CRYAB results in accumulation of MYOC, especially in the insoluble cellular component (Fig. 7, *A* and *B*). Thioflavin T (ThT) staining method can identify misfolded protein aggregates, so we used ThT to stain transfected NTM5 cells. ThT signal was found to be more prominent for mutant MYOC, and the staining was more intense when mutant MYOC was co-transfected with CRYAB (Fig. 7, *C* and *D*). To confirm that mutant MYOC was in the cytoplasm, we transiently-transfected NTM5 cells with cDNA for mutant MYOC Y437H and used a hypotonic lysis buffer to isolate the cytoplasmic fraction. In this experiment, CALR

Figure 4. Mutant MYOC Y435H was not found to adversely impact the rat retina. *A,* averaged waveforms at each stimulus tested. *Arrows* indicate where the pSTR and nSTR amplitudes were measured. No significant differences in ganglion cell function as assessed by the pSTR (-6.0 $p = 0.110$, -5.5 $p = 0.231$, and -5.0 $p = 0.237$) and nSTR (-6.0 $p = 0.998$, -5.5 $p = 0.651$, and -5.0 $p = 0.624$) were observed between 18-month-old WT (*wt*) and mutant Myoc Y435H (*Het*) animals. *B*, averaged scotopic waveforms with *arrows* indicating a- and b-wave measurements. No significant differences in rod/cone photoreceptor function (a-wave, $p = 0.696$) and on bipolar cell function (b-wave, $p = 0.552$) were observed between groups. *C,* representative OCT images; *arrows* indicate thickness measurement. Thickness measurements were made across the entire retinal image excluding the optic nerve region. Retinal thickness as measured from the NFL to the RPE was not significantly different ($p = 0.946$) between groups. Statistical analysis was performed using Student's unpaired *t* test. Abbreviations used are as follows: *ERG,* electroretinogram; *pSTR,* ganglion cell response to low-intensity flash stimuli; *nSTR,* ganglion cell dominated response with contribution from other cell types (*e.g.* amacrine and/or Muller cells).

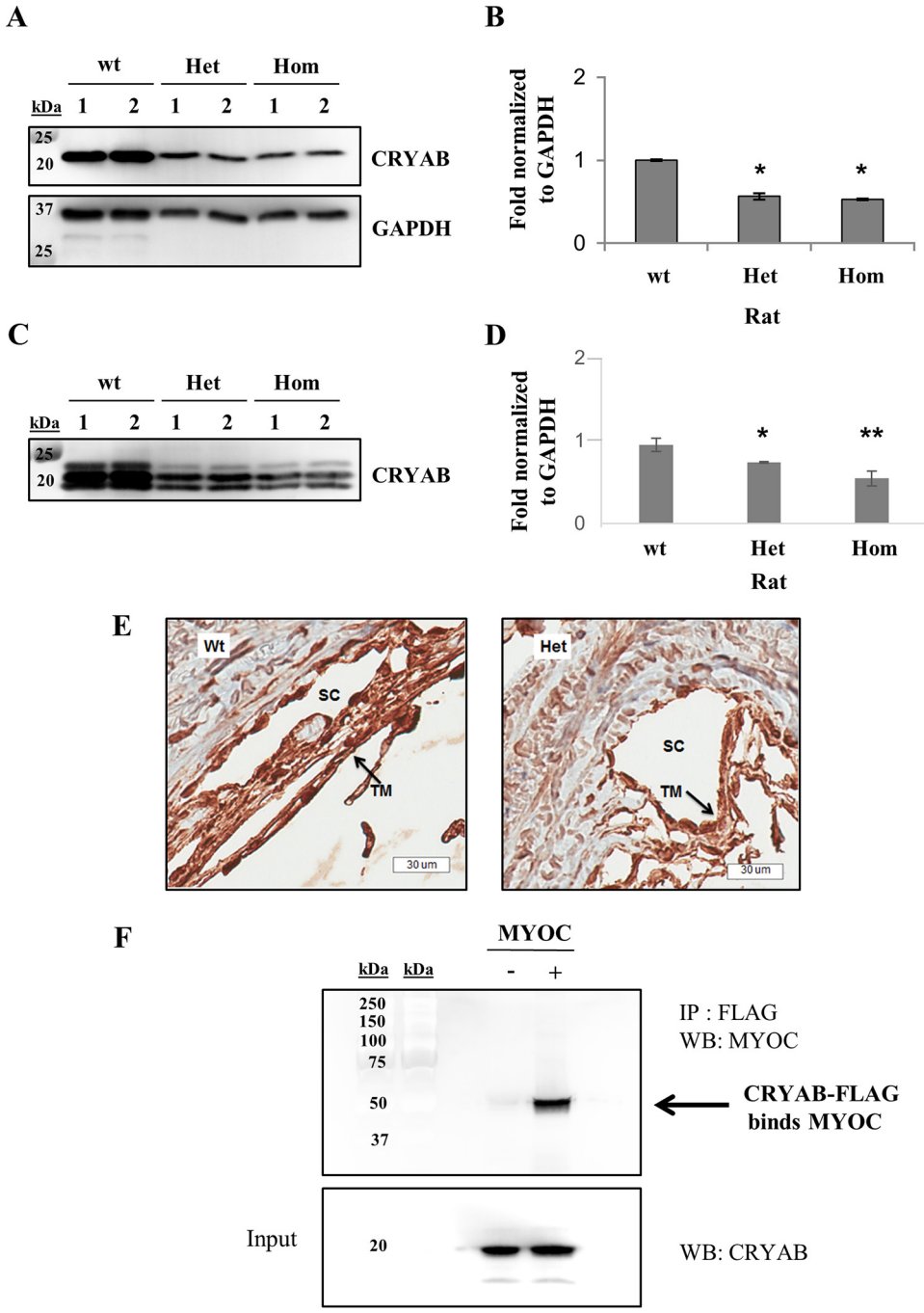

Figure 5. Soluble CRYAB is reduced in rats with a MYOC Y435H mutation, and MYOC has been found to bind CRYAB. *A*, representative Western blottings (*WB*) for CRYAB protein expression in 12-month-old rats indicate that there is more soluble CRYAB detected in WT rat limbal ring lysates compared with MYOC Y435H heterozygote and homozygote rats lysates. 10 μg of each sample was loaded per lane. Representative Western blotting is shown. Quantification of Western blottings indicated approximately 1-fold more soluble CRYAB protein in limbal rings from WT mice compared with rats with the MYOC Y435H mutation. $\pm$ S.D. is indicated. *B*, anti-CRYAB rat limbal ring lysate Western blots were quantified. *Error bars* are $\pm$ S.D., and * indicates *t* test $p < 0.001$. *C*, AH from several different 12-month-old rats were examined for soluble CRYAB protein, and the WT animals had the greatest amount of CRYAB. 10 μg of each sample was loaded per lane. Representative Western blotting is shown. *D*, anti-CRYAB rat AH Western blottings were quantified. *Error bars* are $\pm$ S.D., and * indicates *t* test, $p < 0.05$, and ** indicates *t* test $p = 0.01$. *E*, immunohistochemistry for CRYAB in the trabecular meshwork of 18-month-old WT and heterozygote rats indicates that the WT animals had more detectable CRYAB. *F*, Western blotting results following immunoprecipitation (*IP*) indicate that CRYAB binds MYOC. Abbreviations used are as follows: *Het*, heterozygote; *Hom*, homozygote; *SC*, Schlemm's canal; *TM*, trabecular meshwork; *wt*, WT.

Western blotting serves as a control indicative of ER lumen proteins. Our results do indicate that mutant MYOC is in the cytoplasm, and the probable reason for this finding is because it is being retro-translocated from the ER to the cytoplasm (Fig. 8*A*) and intended for proteasome degradation.

CRYAB is increased in human glaucoma

CRYAB is a heat-shock protein, so its expression is stress-induced. CRYAB expression has been reported to be elevated in the trabecular meshwork in glaucoma (50), and we wished to verify these published findings. What we observed was that

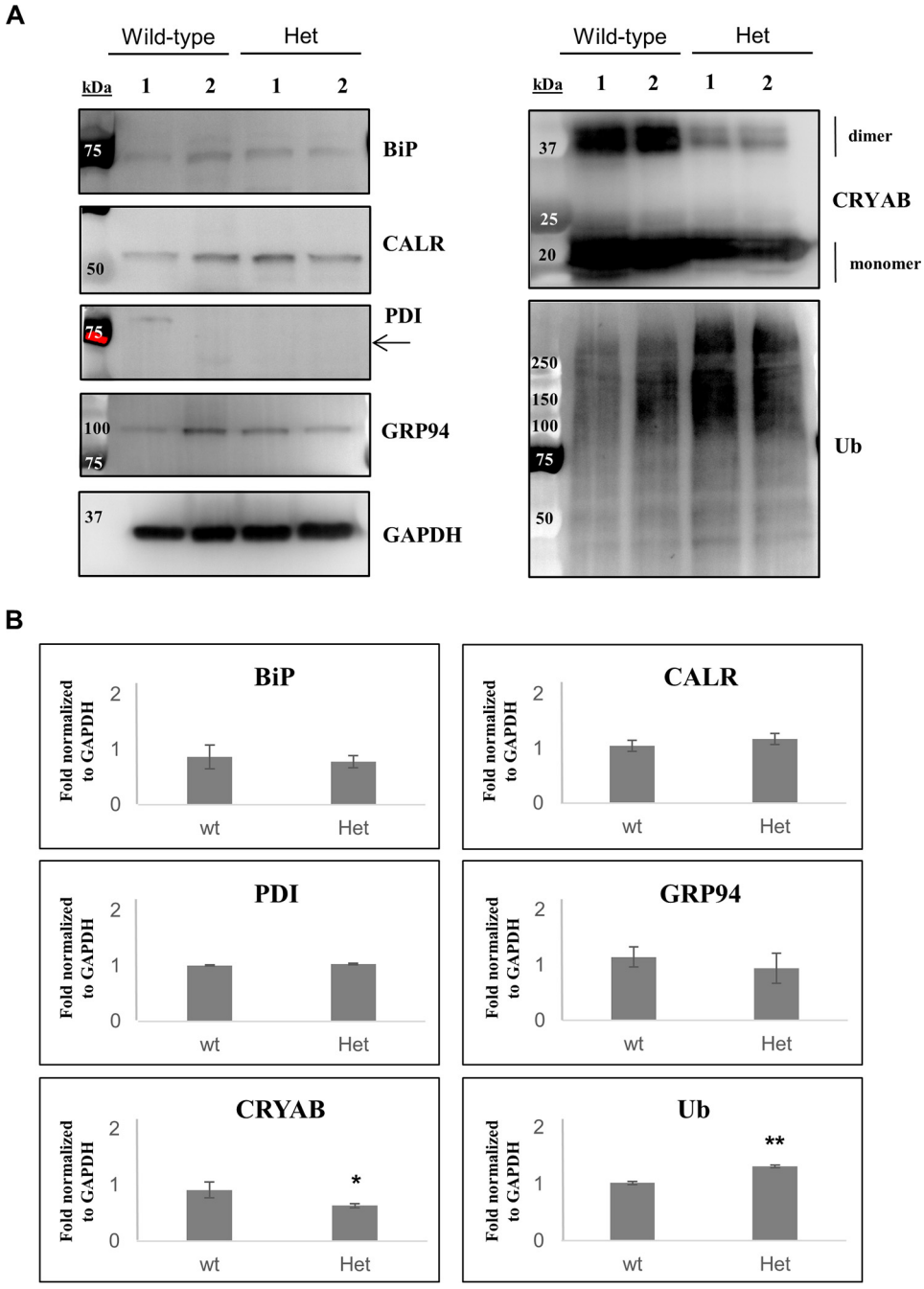

Figure 6. Western blottings for eye lysates from our *in vivo* models show no differences in endoplasmic reticulum proteins, but aged MYOC Y435H heterozygous rats had less soluble CRYAB detected and more high molecular weight Ub proteins. *A*, Western blottings using whole-eye lysates isolated from 18-month-old WT and MYOC Y435H heterozygote rats. *Arrow* indicates expected band location for PDI. *B*, rat whole-eye lysate Western blottings were quantified. *Error bars* are ± S.D. *t* tests for the examined ER proteins showed $p > 0.1$, and * indicates $p < 0.05$ and ** $p < 0.01$. Abbreviations used are as follows: *Het,* heterozygote; *Ub,* ubiquitin; *wt*, WT.

CRYAB, which can be secreted (51), is detectable in human AH following the hypoxia and cell death stresses predicted to occur in cadaver tissues (Fig. 8*B*). We stained human tissue samples for CRYAB protein and observed much higher CRYAB expression in the TM region of the glaucomatous eye compared with the control (Fig. 8*C*). This result was in agreement with the published literature for CRYAB localization in human TM (50). The highest CRYAB expression in the TM appears to be nearest Schlemm's canal in the juxtacanalicular region, which is the site of greatest AH outflow resistance. High CRYAB expression in the juxtacanalicular region has previously been noted (52). Therefore, human glaucoma samples show that there are interesting expression correlations between CRYAB and MYOC. Association of MYOC with CRYAB provides a mechanistic understanding as to how mutant MYOC causes glaucoma (Fig. 9).

Discussion

There are limitations to studying glaucoma in rodent models. In particular, humans have a much more abundant (*i.e.* thicker)

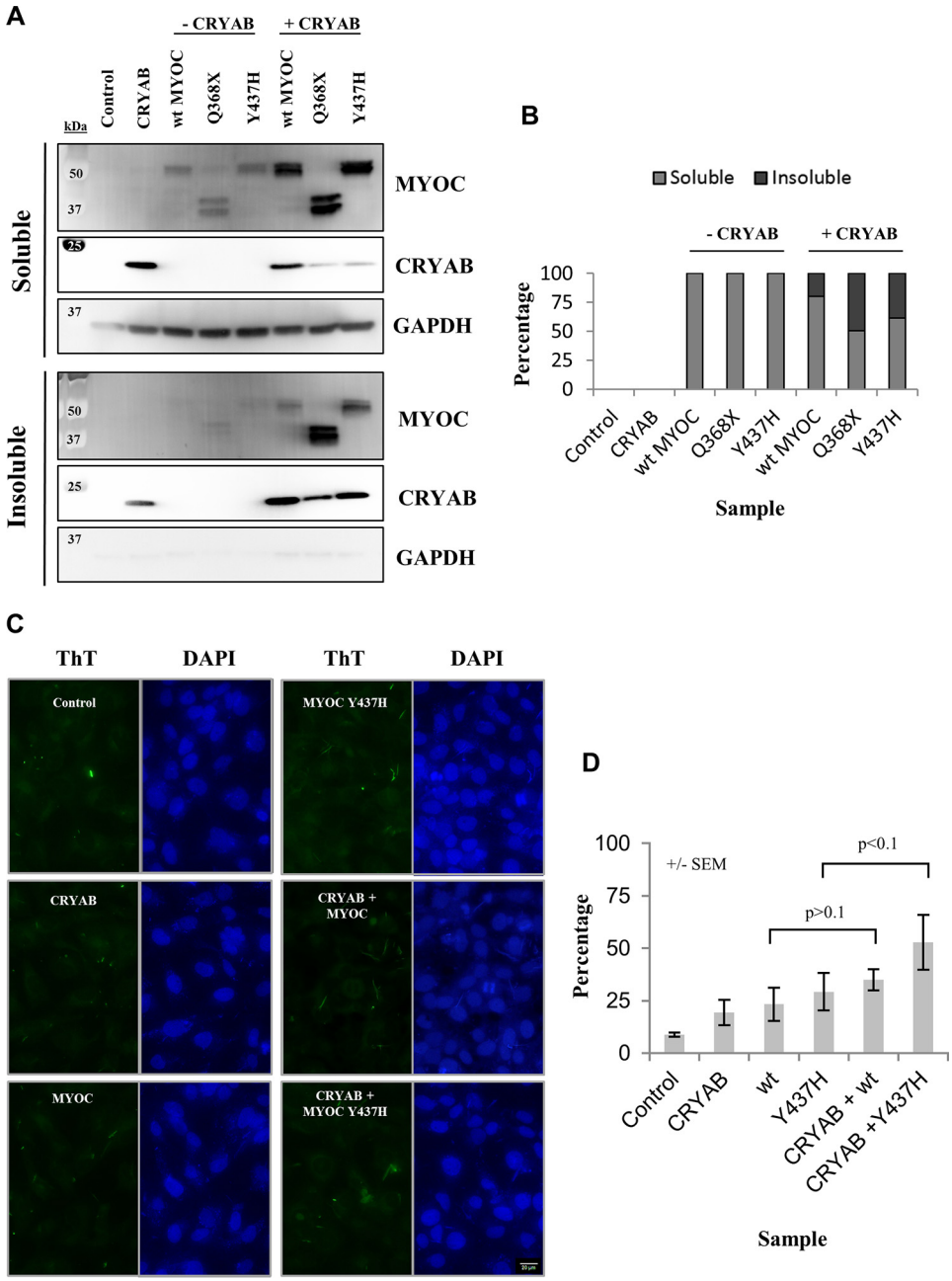

Figure 7. *In vitro*, MYOC protein was found to accumulate in presence of CRYAB. *A,* NTM5 cells were transiently transfected for 48 h with different MYOC cDNAs ± CRYAB and then MYOC in soluble and insoluble fractions examined by Western blotting. Note that very little GAPDH was detectable in the insoluble fraction. *B, bar graph* quantifying anti-MYOC Westerns blottings to show percentage of MYOC in soluble and insoluble fractions. *C,* ThT staining (*green*) for aggregates in NTM5 cells co-transfected with MYOC and CRYAB suggests the most intense staining is when mutant MYOC is co-expressed with CRYAB. The nucleus is counter-stained with DAPI (*blue*). *D,* quantification of number of ThT aggregates relative to cell number ± S.E. and with *t* test results.

TM tissue than rodents (Figs. 1*C* and 5*E*). In addition, humans have ~95% of their AH exiting the eye through the TM and conventional outflow pathway with only 5% of AH exiting via an unconventional mode (53). In comparison, rodents have the majority of their AH (21–83% depending upon strain) exiting the eye through an unconventional pathway (54). These species differences mean that glaucoma pathology may not manifest to the same extent or in a similar relative time in rodents.

Mutant MYOC Y435H rats did not have elevated IOP nor did they have tissue morphology that differed from the WT animals. Similarly, our mutant MYOC Q368X BAC mice did not have an IOP phenotype. MYOC BAC transgenic mice have previously been reported: 1) a transgenic with BAC mouse *Myoc* Y423H mutation (25), which corresponds to the pathological human MYOC Y437H mutation, was reported to have an IOP increase of ~2 mm Hg (OD BAC IOP of 14.1 ± 0.3 mm Hg *versus* WT IOP 12.4 ± 0.3 mm Hg); and 2) a transgenic with BAC human *MYOC* Y437H mutation (26) was reported to have an approximate IOP increase of 2 mm Hg (BAC IOP of 11.8 ± 1.2 mm Hg *versus* WT IOP 10.0 ± 0.8 mm Hg), but this mean IOP increase for the BAC *MYOC* Y437H mouse was later not validated (42). What can be concluded from previously reported BAC myocilin transgenics is that similar results were observed for the animals regardless of whether it was human or

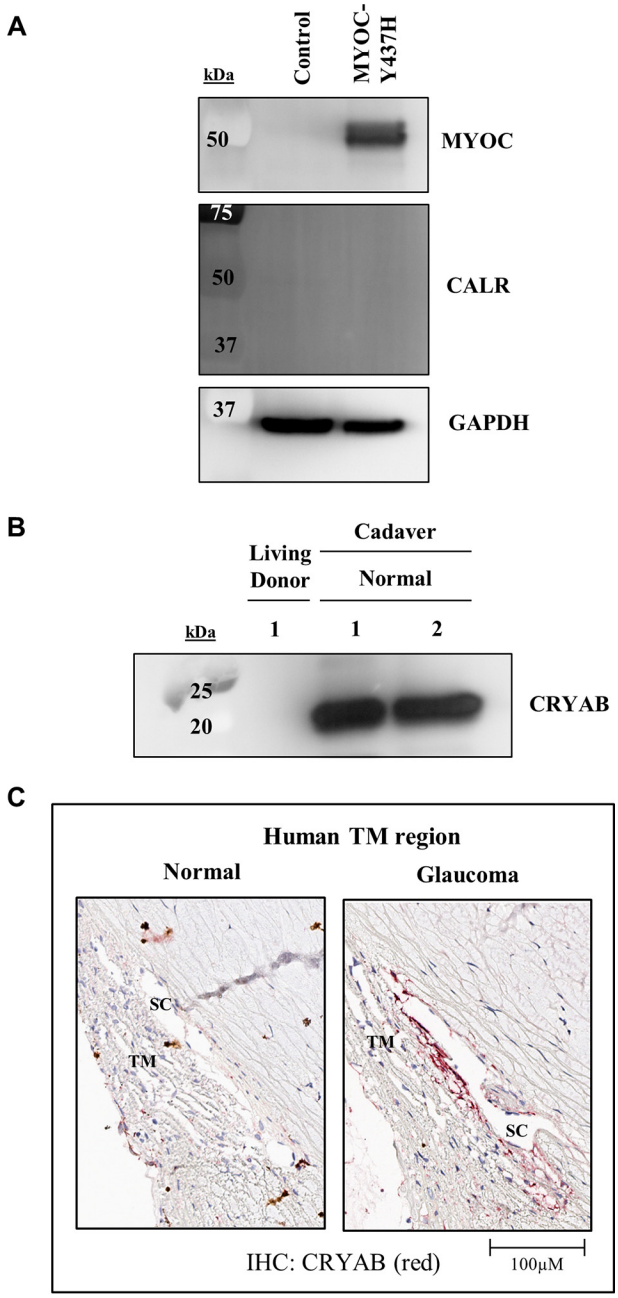

Figure 8. In human AH samples, CRYAB appears following stress conditions. *A,* NTM5 cells transiently transfected for 48 h had cytoplasmic proteins isolated by a hypotonic buffer, and MYOC Y437H was found in the cytoplasmic extract. CALR serves as a control indicating no lysis of the ER. *B,* Western blotting of human donor aqueous humor (10 μg per sample) indicates that CRYAB expression in AH is elevated during stress conditions. *C,* IHC suggests that CRYAB protein (*red color*) is highly expressed in human glaucoma in the trabecular meshwork nearest Schlemm's canal. Nuclei are indicated by hematoxylin staining.

mouse gene utilized. Thus, our IOP findings for our MYOC rodent models are in agreement with what has previously been reported for other myocilin transgenics (25–27).

Despite the lack of an IOP phenotype, differences among WT and mutant MYOC Y435H rats were found via proteomic analysis of rat AH (Table 1). In particular, animals with mutant MYOC Y435H had reduced levels of several crystallin family proteins. Crystallin proteins are highly expressed in the eye where they function as chaperones, protect the cytoskeleton, inhibit apoptosis, enhance resistance of cells to stress, and are neuroprotective (55). There is established precedence in the literature confirming an association between CRYAB levels and disease with CRYAB showing modified expression in glaucoma models of high IOP (56, 57). Additionally, analysis of the human vitreous humor proteome found that expression of numerous crystallin family proteins are significantly down-regulated in glaucomatous eyes (58).

CRYAB is a protein that can be found throughout a cell but also can also be secreted (51). Within a cell, CRYAB functions as a chaperone, where it assists in protein folding as well as helps to shuttle misfolded proteins to the proteasome for clearance (59). Using IP, we verified that MYOC binds CRYAB (Fig. 5*F*), and we further confirmed this interaction using a cell line that has endogenous expression of both MYOC and CRYAB (Fig. S5). In our *in vivo* mutant MYOC models, we observed a decline in soluble CRYAB protein that was accompanied by an intracellular accumulation of HMW ubiquitinated proteins. Accumulation of HMW-ubiquitinated proteins is suggestive of a compromised proteasome and/or impaired protein clearance mechanisms, both of which can have a chronic effect and will eventually impact cell viability.

Both CRYAB and MYOC are highly expressed in the TM. Normally, these small MYOC–CRYAB protein complexes within the cytoplasm should be effectively cleared by the proteasome; however, under stress conditions, TM cells produce elevated amounts of both MYOC and CRYAB, and protein accumulation may occur. We observed this protein accumulation in NTM5 cells co-transfected with mutant MYOC and CRYAB as evidenced by ThT staining (Fig. 7*C*). One function of CRYAB is to inhibit amorphous (disordered) aggregation by participating in amyloid fibril formation that leads to ordered β-sheet–containing aggregates (60). We postulate that in the short term, binding of MYOC to CRYAB may be beneficial to the TM cell by facilitating a recovery process. Binding of CRYAB to misfolded mutant proteins has been shown to aid in the restoration of cellular homeostasis and even an extended lifespan (61, 62). However, if the aggregates are not efficiently cleared by the proteasome then the aggregates pose a long-term threat to cell vitality (55). This idea is supported by the observation that fewer TM cells are present in trabeculectomy samples from mutant MYOC donors (63).

Protein folding in the ER is not completely efficient (64), so some misfolded WT proteins will normally occur. Misfolded protein is regularly retro-translocated from the ER into the cytoplasm for degradation via a process known as ER-associated degradation (ERAD). ERAD can utilize the ubiquitin–proteasome pathway, and MYOC has previously been shown to be cleared by the proteasome (65). When mutant MYOC is the protein being produced, then large amounts of misfolded MYOC protein will begin to accumulate, and it will associate with CRYAB within the cell. It has been observed that for cytoplasmic aggregates, such as that observed for mutant desmin protein, there is a feedback on ERAD resulting in a mild ER-signaling response (66). Thus, it is possible that the ER stress response reported by some researchers (34, 67) for mutant MYOC proteins may arise as an artifact of overexpression or as a secondary response to the primary event of cytoplasmic pro-

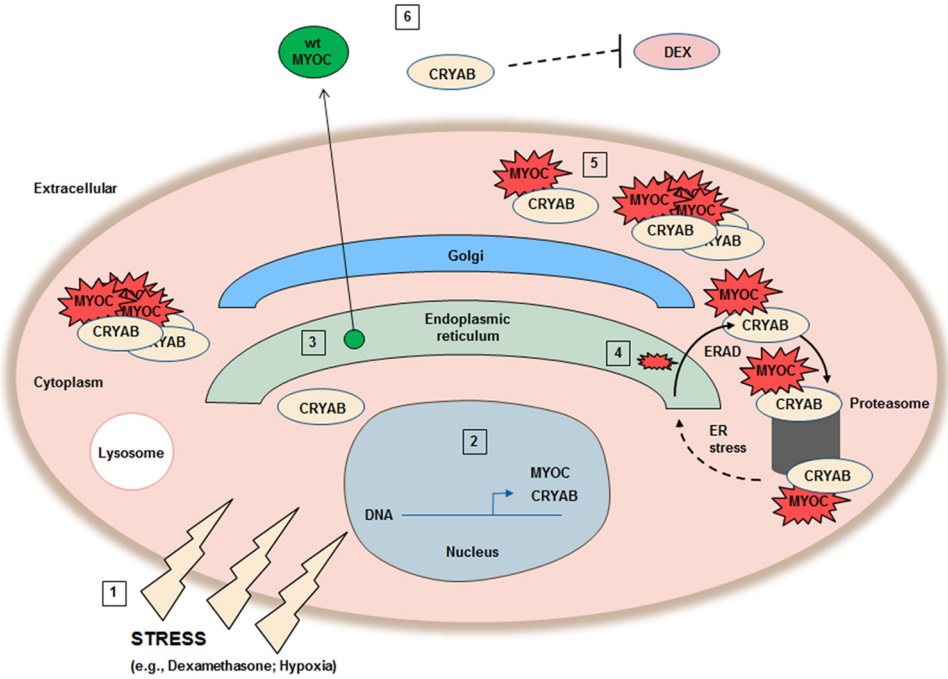

Figure 9. Cartoon figure of a cell illustrating simplified mechanism of mutant MYOC-induced glaucoma pathology. *Step 1*, stresses will result in *step 2*, activation of *MYOC* and *CRYAB* gene expression. *Step 3,* WT MYOC (*dark green*) is synthesized in the ER and is a secreted matricellular protein. *Step 4,* in the case of mutant MYOC (*red*), it is misfolded and will be retro-translocated from the ER to the cytoplasm for clearance by ERAD, which utilizes the proteasome. In the cytoplasm, mutant MYOC can bind CRYAB. Increased stress as well as time/age will result in diminished efficiency of protein clearance, and this will impact ERAD with feedback signaling to the ER occurring so as to mildly increase expression of ER and ERAD proteins to try and correct the problem. *Step 5,* with time/age mutant MYOC protein aggregates will accumulate within the cell. These aggregates can compromise cell function and threaten/impact cell viability. Thus, MYOC-induced glaucoma is a protein misfolding disease, and pathology occurs in a manner similar to other aging diseases. *Step 6,* outside the cell WT MYOC likely acts as a matricellular protein and may have other functions, but additional research is required. Crystallin has been reported (73) to bind and inhibit dexamethasone. Abbreviation used is as follows: *DEX*, dexamethasone.

tein aggregates and inefficient protein clearance. Hence, when protein expression is within physiological relevance, the ER stress is a secondary and not a primary cause of mutant MYOC pathology. Proteins prone to aggregation typically have high β-sheet content (68), and MYOC OLF domain is a five-bladed β-propeller (33, 69). It would be interesting to know whether protein aggregation results in glaucoma for other GLC1 proteins (*e.g.* GLC1G/WDR36 which contains two multibladed β-propellers). In addition, it would be interesting to investigate whether protein aggregation and/or CRYAB binding is a universal feature in this multifactorial disease.

Our proposed model for mutant MYOC pathology is supported by published *in vivo* data. A mouse model with mutant MYOC Y437H expression under control of a lens-specific crystallin promoter (27) was found to develop cataracts by 6 weeks of age, and the lenses of these transgenics eventually ruptured. The lens is extremely enriched in crystallin proteins, so this animal model supports our findings that co-expression of mutant MYOC with CRYAB can adversely impact a cell eventually leading to cell death. Interestingly, CRYAB and MYOC: 1) are expressed in the same limited number of tissues, which include the eye, heart, and skeletal muscle (21, 34, 70); 2) both are stressed-induced genes (70); 3) both are up-regulated following steroid (*e.g.* dexamethasone) treatment (38, 71); and 4) both have expression enhanced in the presence of soft substrates/matrices (72). Extracellular crystallin has been reported to bind dexamethasone (73), and as both *MYOC* and *CRYAB* gene expression are up-regulated by dexamethasone, this potentially identifies a feedback for our MYOC model (Fig. 9).

Current information in the literature that challenges our proposed model for mutant MYOC is a publication that reported that only heterozygotes in a mutant MYOC K423E pedigree, not homozygotes, developed glaucoma (11). This 2-decade-old *MYOC* publication is the only example in the literature of a hypothetical form of simple inheritance (74). Since that early MYOC publication, several people homozygous for pathological MYOC mutations have been reported as having glaucoma (63, 75). In fact, homozygotes for MYOC T377M have a more severe glaucoma phenotype than MYOC T377M heterozygotes (75). Typically, in the case of a pathological misfolded protein, one would expect that: 1) homozygotes would have a more severe phenotype than heterozygotes; and 2) offspring carrying two pathological variants on opposing alleles would also have a phenotype more severe than heterozygotes with a single mutation. The researchers that reported the MYOC K423E pedigree (11) later acknowledged that a spouse in the K423E pedigree carried mutant MYOC R126W and their blind child, who had the most severe phenotype in the family tree, carried both MYOC variants (76). In another reported pedigree, individuals that were compound heterozygotes for mutant MYOC Q368X and mutant MYOC T377M were found to have a more severe glaucoma phenotype than people with either mutant alone (77). Therefore, there are examples in the literature that challenge the idea that homozygotes for mutant MYOC do not manifest glaucoma. Our data from our MYOC Y435H rat model suggest that heterozygote and homozygote rats are more similar to each other and different from the WT animals. One can speculate that the report for the MYOC

K423E homozygotes was at an age before the glaucoma disease onset; alternatively, there may be a *MYOC* gene penetrance variable to consider and/or external stress factor(s) needed to enhance *MYOC* gene expression to manifest glaucoma.

Protein aggregates can initiate cell dysfunction to impact cell viability (60), and aggregates are well-established as a factor in several age-related diseases (60, 78). Interestingly, patients with Alzheimer's disease have a higher risk of glaucoma, and optic nerve changes have also been shown in patients with Parkinson's disease (79). The predominant current hypothesis is that mutant MYOC causes glaucoma pathology through a mechanism involving intracellular accumulation of misfolded protein (47, 80). Herein, we have identified CRYAB as a MYOC binder. We show that severity of aggregates is enhanced when the two proteins are co-expressed. Changes to the level of available CRYAB can cause cell dysfunction by compromising efficiency of the ubiquitin–proteasome pathway (70). Aggregation of CRYAB with MYOC also prevents CRYAB from performing its numerous normal essential cellular functions, which include 1) a chaperone (55, 59); 2) a protein important for inhibiting apoptosis (81); and 3) a protein providing neuroprotection (82). Thus, intracellular binding of MYOC to CRYAB will impact cell homeostasis, and the aggregates could cause disease development and/or progression.

Up-regulation and aggregation of WT MYOC has been reported in other glaucoma subtypes, and this suggests broader relevance of misfolded MYOC across the disease spectrum (80). To date, methods to target misfolded MYOC have focused on MYOC in the ER (80), but a limitation to this strategy is that it does not address aggregation of MYOC in the cytoplasm. The relevance of our identification of the MYOC–CRYAB interaction is that it supports therapeutic approaches to prevent cytoplasmic MYOC aggregates that compromise the ERAD pathway. We postulate that disruption of the MYOC–CRYAB interaction will assist in protein clearance thus preventing TM cell dysfunction and the resulting cell death that occurs in glaucoma. A compound that targets CRYAB has been reported (84), and future research may involve studying the application of this or other CRYAB-targeting compounds in a model that is representative of the patient with a pathological *MYOC* mutation.

POAG is a disease associated with aging. Many aging diseases, such as Alzheimer's, Parkinson's, and Huntington's, have pathology attributed to chronic accumulation of misfolded proteins that will eventually compromise cell function and viability. Our finding that MYOC binds CRYAB adds to the biological understanding how pathological MYOC mutations cause glaucoma. As rodents have a much smaller TM region than humans, the majority of their AH exiting via an unconventional pathway, and only an approximate 2-year life span, it can be concluded that no currently available rodent model ideally represents the chronic nature of human POAG. As such, all current *in vitro* and *in vivo* myocilin rodent models for POAG have limitations. An effort to establish or identify an *in vivo* model that better resembles human POAG is paramount to advancing the development of novel glaucoma treatments to directly modify disease pathology. The application of CRISPR/Cas9 technology provides researchers with new opportunities to develop these novel *in vitro* and *in vivo* models to better study MYOC and its role in POAG.

Two decades post-discovery, *MYOC* remains a fascinating gene that is strongly-associated with glaucoma. We propose that targeting *MYOC* at a transcriptional or transcript level to reduce the amount of MYOC protein or, alternatively, a low molecular weight compound that reduces MYOC–CRYAB protein complexes/aggregates may be potential therapeutic approaches. Discovery of the MYOC–CRYAB complex provides new insight as to how mutant MYOC is causing pathology via the removal of CRYAB from performing its many prosurvival cellular functions. It is hoped that identification of this complex will assist in facilitating a treatment strategy to help the patient with a pathological *MYOC* mutation so that these patients may retain their vision and maintain quality of life.

Materials and methods

Human samples

Human samples were obtained with consent from regional donor eye banks. AH from living donors was collected during cataract surgery and immediately frozen, while AH and tissues collected from cadaver donor eyes were collected $<$12 h post mortem and immediately frozen upon isolation. All human samples were stored at −80 °C until use. Medical histories provided patient information. All human samples were from donors of a similar elderly age. Note that none of the human donors had a *MYOC* mutation.

Animal models

All procedures in this investigation conformed to the Association for Research in Vision and Ophthalmology (ARVO) resolution on the Use of Animals in Ophthalmic and Vision Research and were reviewed and approved by the Institutional Animal Care and Use Committee (IACUC) at Novartis Institutes for Biomedical Research. Animals were housed in rooms in which the temperature, humidity, and lighting (12:12 h light/dark cycle) were controlled, and water and food were available *ad libitum*. When animal tissues samples were collected, they were immediately frozen and then stored at −80 °C until used.

CRIPSR-engineered MYOC Y435H mice

CRISPR-engineered Sprague-Dawley MYOC Y435H rats were created by Horizon Labs (St. Louis, MO), and the *Myoc* gene was sequenced to ensure only the single mutation was introduced. To identify the rats as WT (native), heterozygote, or homozygote for the MYOC Y435H mutation, genomic DNA was isolated from tail clippings. Tails were digested in 1× Tail Buffer (10 mM Tris, pH 8; 2.5 mM EDTA; 100 mM NaCl; 0.1% SDS) with proteinase K (10 mg/ml) added. Genomic DNA was purified by a single precipitation step using phenol/chloroform/isoamyl. The isolated genomic DNA was amplified by PCR using rat Myoc primers (forward: 5′-ctgtggatgagagcggcctc-3′, and reverse: 5′-gtgaccatgttgaagttgtcc-3′). For PCR, GeneChoice polymerase (Apex, 42-409R) and a C1000 Touch™ thermal cycler (Bio-Rad, 52 °C annealing and 72 °C extension temperatures) were utilized. PCR products (343 bp) were gel-purified from 0.8% agarose/1× TAE gels using a gel

purification kit (Qiagen, 28704) according to the manufacturer's instructions. Sequencing was completed by GeneWiz (Cambridge, MA) using the forward Myoc primer. Animals were born at expected Mendelian frequencies, and no breeding or viability issues were noted. All experimental animals were obtained from heterozygote breeding pairs.

MYOC WT BAC and MYOC Q368X BAC mice

BAC containing the human *MYOC* gene (RP11-1152G22) was used to generate the transgenic mouse lines. This BAC contains the entire MYOC coding sequence, with 68-kb 5′- and 51-kb 3′-flanking sequences. Modification of the BAC to introduce the C>T mutation at position 1102 of the coding sequence was performed by GeneBridges (Heidelberg, Germany). Purified BAC constructs were injected into the pronuclei of C57BL/6J mice. The resulting offspring were screened by PCR to identify transgenic founders, and one founder for each of the WT BAC and mutant BAC was used to establish transgenic lines. No breeding complications or viability issues were noted for any of the mice.

Measurement of conscious IOP

Animals underwent training of conscious IOP measurement for more than 3 weeks. IOP was measured with a TonoLab rebound tonometer (Colonial Medical Supply, Franconia, NH) twice per week at the same time each mid-day. Ten measurements deemed reliable by internal software were utilized to generate and display an average. An average of these readings was then calculated and reported as mean IOP ± S.E. The normal variability expected for multiple examiners using tonometers is ~1 mm Hg (85).

Implantation of prednisolone or placebo pellet

IOP was monitored in the rat cohorts before and after prednisolone challenge. Each animal cohort consisted of 10 WT, 10 heterozygote, and 10 homozygote animals. Pellets were ordered from Innovative Research of America (Sarasota, FL), and the prednisolone pellet was 25 mg × 60 days releasing. Animals were anesthetized with an i.p. injection of a mixture of ketamine (35 mg/kg) and xylazine (5 mg/kg). Subcutaneous implantation was conducted via small incision in the dorsal neck area. RT-PCR using Myoc rat primers (ThermoFisher Scientific, Rn00578382_m1) suggested that Myoc transcript increased up to six times with prednisolone treatment.

Electroretinography methods

Electroretinography (ERG) was performed using the Espion™ E3 system (Diagnosys LLC, Lowell, MA) equipped with dual Colordome Ganzfeld stimulators. ERGs were acquired from Sprague-Dawley MYOC Y435H rats ($n = 9$) and WT Sprague-Dawley rats ($n = 6$). Preceding the recording, the animals were dark-adapted overnight in a ventilated light-tight enclosure (Phenome Technologies) for at least 18 h. Pupils were dilated using 1–2 drops of 1.0% cyclopentolate hydrochloride (Alcon) and 1–2 drops of 2.5% phenylephrine hydrochloride (Akorn). Proparacaine 0.5% (Akorn) was applied topically as a local anesthetic. Rats were subsequently anesthetized with an intraperitoneal injection of a ketamine/xylazine mixture (75.0:5.0 mg/kg) and positioned on a warm-water heating pad during the recording. Corneal hydration was maintained through application of 1.0% carboxymethylcellulose lubricating drops (TheraTears, Akorn). ERGs were recorded using a gold loop contact lens electrode (LKC, part no. R275) referenced to a gold nasopharyngeal electrode (Natus Technologies, F-ERG-G) placed in the mouth. A 30-gauge platinum electrode was inserted subcutaneously in the tail to ground the recording. All procedures were performed under dim red illumination (>650 nm). The scotopic threshold responses were elicited with −6.0, −5.5, and −5.0 log cd·s/m^2 flash luminance (50 replicate flashes, 2-s interstimulus interval). Photoreceptor (a-wave) and on-bipolar cell function (b-wave) were assessed by a single 2.2 log cd·s/m^2 high luminance stimulus. ERG traces were analyzed using a customized script written in MATLAB (Mathworks, Natick, MA). Data quantification and statistical analysis were performed using GraphPad Prism (Version 7).

OCT

Ocular imaging was performed using a spectral domain OCT imaging system (Leica Microsystems, Bioptigen Envisu R2210). Anesthesia and pupil dilation were performed as stated in the ERG protocol. Corneal hydration was maintained through application of 0.3% hypromellose lubricating drops (Alcon). OCT b-scans centered on the optic nerve were acquired in the inferior–superior (vertical scan) and nasal–temporal (horizontal scan) directions from each eye. Ten 1.8-mm b-scans were acquired at each position and then subsequently aligned and averaged for analysis. Retinal thickness assessments were performed using a custom code developed in MATLAB (Mathworks Release 2016a). The central 200-μm centered on the optic nerve head was excluded from the thickness measurements to avoid alignment variability observed near the optic nerve. Total retinal thickness measurements were performed manually by delineating the NFL and RPE/Bruch's membrane. Retinal thickness measurements from both eyes were averaged for each animal. Statistical analysis and graphing were performed using GraphPad Prism (Version 7).

Histology

Human anterior segments, rat eyes, and mouse eyes were all fixed in 10% neutral-buffered formalin for 3–4 days (human and rat) and 2 days (mouse). The tissues were processed for paraffin embedding in Tissue-Tek VIP and Tissue-Tek Tec (Sakura). Paraffin blocks were sectioned (5 μm) and mounted to slides (Superfrost Plus, ThermoFisher Scientific). Slides from each eye were treated with antibody and/or stained with H&E or trichrome in accordance with auto-staining machine protocols (Tissue-Tek Prisma®, Sakura).

Immunohistochemistry was run on LeicaBond Rx IHC/ISH slide staining system. Slides were treated by heat-induced epitope retrieval ER2 (pH 9.0, AR9640) for 20 min. Primary antibodies were incubated for 30 min. Specifically bound antibodies were visualized using Bond Polymer Refine Detection System (Leica, DS9390). Finally, stained slides were covered and scanned into Aperio AT2 slide scanner (Leica).

Primary antibodies and working concentrations were as follows: 1) rabbit anti-MYOC 0.2 μg/ml (Sigma, HPA027364); 2)

mouse anti-CRYAB 0.2 μg/ml (Abcam, ab13496); 3) mouse α-smooth muscle actin (α-SMA) 1 μg/ml (Abcam, ab7817); 4) rabbit anti-collagen IV (COLIV) 2 μg/ml (Millipore, AB756p, 1 mg/ml); and 5) rabbit anti-fibronectin (FN1) 0.18 μg/ml (Proteintech, 15613-1-AP).

In vitro experiments

An immortalized human normal trabecular meshwork cell line 5 (NTM5) was utilized, and this cell line has previously been described (86). MYOC is a protein whose expression in primary cells declines with culture time (87). Additionally, NTM5 cells no longer express MYOC protein nor is the MYOC protein level in NTM5 cells impacted by dexamethasone treatment. NTM5 cells were grown in 10-cm culture dishes in a 37 °C incubator with 90% relative humidity and 5% CO_2. Cell media used for NTM5 cells were DMEM (Gibco, 1199-065) supplemented with 10% FBS (Gibco, 10082147) and 1% penicillin/streptomycin (Gibco, 15140-122). NTM5 cells at 70–80% confluence were transiently transfected with plasmids (6 μg of total cDNA per 10-cm plate) using FuGENE 6 transfection reagent (Promega, E2691). Human MYOC plasmids were all in the same vector, which had a minimal CMV promoter. CMV–MYOC plasmid cDNAs had been created and sequences confirmed by GeneWiz. One plasmid contained cDNA for WT untagged MYOC (accession no. NM_000261), and the other plasmids had cDNA for mutant MYOC with either the Y437H mutation or Q368X mutation. Additional plasmids included human CRYAB (Origene, RC202718; accession no. NM_001885). All plasmids had been purified using a Qiagen plasmid maxi kit (Qiagen, 12163), and for transfections FuGENE 6 was utilized at a 5:1 ratio with the cDNA. 48 h post-transfection, cells were washed with 1× PBS (Gibco, 20012-027) and lysed on ice using a RIPA buffer (50 mM Tris (pH 7.5), 150 mM NaCl, 1 mM EDTA (pH 8.0), 1 mM EGTA (pH 8.0), 0.1% SDS, 1% Triton X-100, 0.5% sodium deoxycholate, 1 mM DTT) with Complete protease inhibitors (Roche Applied Science, 11873580001). Cell debris was removed by cold centrifugation (Eppendorf 5810R), and the soluble cell lysates in the supernatant were retained. Protein assay (Bio-Rad DC kit, 500-0113, 500-0114, and 500-0115) was completed in accordance with the manufacturer's instructions using a Tecan Infinite M1000 plate reader with Tecan i-Control 3.1.9.0 software.

To protein samples, 5× SDS loading buffer (0.25 M Tris (pH 7.0), 40% glycerol, 8% SDS, 20% β-mercaptoethanol, 0.1% bromphenol blue) was added, and Western blot analysis was completed using 10% SDS-polyacrylamide gels (Bio-Rad Mini-PROTEAN TGX gels, 456-1034) in the Bio-Rad Mini-Protean Tetra System followed by wet transfer to polyvinylidene difluoride membranes (Millipore, IPVH00010). Membranes were blocked using a solution of 5% powdered nonfat milk in 1× TBS-T. Membranes were treated with primary antibody (1:1000 in a solution of 1% nonfat milk and 1× TBS-T) with gentle rocking overnight at 4 °C. After incubation in primary antibody, membranes were washed with 1× TBS-T followed by 90-min room temperature incubation with species-appropriate AP-conjugated secondary antibody (Abcam). Following 1× TBS-T washes, membranes were exposed to ECF substrate (VWR, RPN5785) and imaged using a Bio-Rad GelDoc XR+ Imaging System with ImageLab 5.2.1 software. Quantification of Western blots was performing using the GelDoc software.

Isolation of in vitro protein fractions

NTM5 cells in 10-cm culture dishes were transiently transfected with FuGENE 6 as described. The control vector was CMV-Tag1 (Agilent, 211170), and the CMV–MYOC plasmid cDNAs had been created by GeneWiz. 24 h post-transfection, cells were washed five times with 1× PBS, and 10 ml of serum-free DMEM was added to each plate. 48 h post-transfection, cell fractions were harvested. For isolation of secreted *in vitro* protein, serum-free media were collected and centrifuged at room temperature for 5 min at 1000 rpm to pellet any debris. Supernatants were retained, and then samples were concentrated 100× using cold centrifugation and Ambion Ultra-4 Centrifugal Filters (Millipore, UFC801008). Protein concentration was determined by the Bio-Rad DC protein assay, and samples were analyzed by Western blotting. For Western blotting, 5× SDS loading buffer was added to each sample. For isolation of soluble cell lysates, a minimal amount of RIPA buffer with protease inhibitors was added to each plate, and the plates were placed on ice for 10 min. Cells were scraped from the plates using a cell scraper (Corning, 3008), and the samples were transferred to pre-chilled tubes. Tubes were centrifuged at 4 °C for 10 min at 7500 rpm. The supernatant (soluble fraction) was isolated and saved in tubes on ice, and the pellet was processed as described below. Bio-Rad DC protein assay of the soluble samples was completed. 5× SDS loading buffer was added to each sample, and samples were placed in a boiling water bath for 5 min. For isolation of insoluble cell lysates to the pellet of each sample, 250 μl of RIPA buffer with protease inhibitors was added, and these samples were briefly sonicated three times (Misonix XL-2000, 7 V). 100 μl of 5× SDS loading buffer was added to each of these samples, and the tubes were placed in a boiling water bath for 5 min. RIPA buffer was added to the insoluble samples to equalize the volume to that in the soluble fractions.

Isolation of in vivo protein

Tissue harvested from animals was minced with scissors and homogenized (Omni Tissue Master 125 Homogenizer, Omni International) in the RIPA buffer with Complete protease inhibitors (Roche Applied Science). The tissue samples were sonicated using a Misonix Sonicator XL-2000 series with ultrasonic converter (Serial C6498) set at power setting 1 (5 V). Samples were cold-centrifuged and supernatants saved. Sample protein concentration was determined by the Bio-Rad DC protein assay. For Western blotting, 5× SDS loading buffer was added to each sample, and samples were placed in a boiling water bath for 5 min before being loaded into wells of 10% SDS-polyacrylamide gels.

Antibodies

All primary antibodies were from commercial sources. With the exception of anti-GAPDH (1:10,000), and unless otherwise mentioned, all primary antibodies for Western blotting application were typically utilized at a 1:1000 dilution in 1% nonfat milk and 1× TBS-T. All primary antibody incubations were overnight at 4 °C with gentle rocking. Primary antibodies uti-

lized in this study for Western blotting and for histology applications were as follows: ARMET (Abcam, ab126321), BIP (Cell Signaling Technology, 3183S), CALR (Cell Signaling Technology, 2891S), CRYAB (Abcam 76467), CRYAB for IP (Cell Signaling Technology, 45844), FLAG (Sigma, F1804), GAPDH (Fitzgerald, 10R-G109a; 1:10,000), GRP94 (Cell Signaling Technology, 2104S), MYOC (Acris, AP10162PU-N), MYOC (Origene, TA323708), MYOC (R&D Systems, AF2537; 1 μg/μl), MYOC (Sigma, HPA027364), and ubiquitin (Abcam, ab134953). For Western blotting, all secondary antibodies were AP-conjugated and were utilized at a 1:2000 dilution in 1% nonfat milk and 1× TBS-T. All secondary antibodies were purchased from Abcam (ab97107, ab97237, and ab6722). As a Western blotting loading control, membranes were stripped according to the manufacturer's instructions using 1× Strong Stripping Buffer (Millipore, 2504) and after blocking in a 5% nonfat milk, 1× TBS-T solution, the membranes were treated with anti-GAPDH.

Gel LC MS-MS analysis of rat aqueous humor

Upon separation of pooled rat aqueous humor samples by SDS-PAGE and staining with SimplyBlue (Invitrogen, LC6065), protein bands were excised from gels and subjected to trypsin digestion. Trypsin digestion was performed according to standard procedures (88). Briefly, the gel pieces were dehydrated with acetonitrile (ThermoFisher Scientific) and rehydrated with 100 mM NH_4HCO_3 buffer containing 10 mM DTT (ThermoFisher Scientific) to reduce disulfide bonds. Gel pieces were treated with 100 mM NH_4HCO_3 buffer containing 20 mM iodoacetamide (ThermoFisher Scientific) to alkylate cysteines. After two rounds of dehydration with acetonitrile and rehydration with 100 mM NH_4HCO_3 buffer, the dried gel pieces were rehydrated with 20 ng/μl trypsin sequencing grade (Roche Applied Science) in 50 mM NH_4HCO_3 buffer and incubated overnight at 37 °C. Peptides were extracted with 75% acetonitrile, 0.1% formic acid and dried in a vacuum centrifuge. Samples were resuspended in 5% acetonitrile, 0.1% formic acid and introduced to an Orbitrap Fusion Lumos (ThermoFisher Scientific) using an EASY nano-LC1200 system (ThermoFisher Scientific) with an analytical column packed with a 0.075 × 200 mm ReproSil-Pur C18-AQ, 3 μm (Dr. Maisch, Ammerbuch, Germany).

MS and tandem MS/MS spectra were performed on an Orbitrap Fusion Lumos mass spectrometer operated on data-dependent acquisition mode. Survey MS1 scans were acquired in the Orbitrap using a 350–1400 m/z range at 120,000 resolution. The most intense ions per survey scan (top speed mode), rising above threshold, were selected for HCD fragmentation, and the resulting fragments were analyzed in the Orbitrap. Proteome Discoverer software suite (Version 2.1, ThermoFisher Scientific) was used for peptide identification. The data were searched against the UniProt rat database (Version Nov., 2015). At the MS1 level, a precursor ion mass tolerance of 10 ppm was used, and up to three missed cleavages were allowed. The fragment ion mass tolerance was set to 20 millimass units (mmu) for the Orbitrap MS/MS detection methods. Oxidation of methionine was defined as a variable modification, and carbamidomethylation on cysteines was defined as a fixed modification. False discovery rate in peptide identification was limited to a maximum of 0.01 by using a decoy database. Abundance data were retrieved from the "Precursor ion area detector" node from Proteome Discoverer (Version 2.0) using 2 ppm mass tolerance for the peptide extracted ion current.

Immunoprecipitation

NTM5 cells were grown in 10-cm culture dishes and were transiently transfected. Plasmid cDNAs utilized were for WT untagged MYOC (accession no. NM_000261) and CRYAB-FLAG (Origene, RC202718, accession number NM_001885), and the control vector was pCMV-Tag1. 24 h post-transfection, plates of transfected cells were washed five times with 1× PBS, and 10 ml of serum-free DMEM was added to each plate. 48 h post-transfection, the media were collected from these plates and concentrated to 100× using Ambion filter units. Similar media samples were pooled, and protein concentration was determined by the Bio-Rad DC protein assay.

48 h post-transfection, the NTM5 cells were washed with 1× PBS and then 250 μl of IP buffer (20 mM Tris-HCl (pH 7.5), 150 mM NaCl, 1 mM EDTA, 1 mM EGTA, 1% Triton X-100) with Roche Applied Science Complete protease inhibitors was added to each plate for 10-min incubation on ice. Cell lysates were transferred into tubes and sonicated once at power setting 1 (5 V) for 15 s. Tubes were then centrifuged at 7500 rpm at 4 °C for 10 min, and the supernatants were transferred to new pre-chilled tubes. Similar samples were pooled, and Bio-Rad DC protein assay was completed. 50 μl of anti-FLAG antibody was added to each tube, and tubes were incubated overnight at 4 °C with gentle rotation. Later, 40 μl of Pierce protein A/G-agarose (ThermoFisher Scientific, 20241) beads were added to each tube for a 90-min incubation at 4 °C with gentle rotation. Using the cold centrifuge (1000 × g at 4 °C for 3 min), samples were gently centrifuged to pellet the A/G beads. Beads were washed five times with the IP buffer, and then 15 μl of 5× SDS loading buffer added. Sample tubes were placed in a boiling water bath for 5 min and then centrifuged at room temperature at 13,000 rpm for 3 min. The supernatant was retained for Western blot analysis. This IP protocol is a modified version of that provided by Cell Signaling Technology for native proteins.

The Broad Institute Cancer Cell Line Encyclopedia was searched to identify immortalized human cell lines with high transcript levels of both MYOC and CRYAB (https://portals.broadinstitute.org/ccle).[3] Two soft tissue cell lines were identified (Fig. S5*A*) from the CCLE of which the G401 cell line was chosen for IP experiments. G401 cells were grown in McCoy's 5A media (Gibco, 16600082) supplemented with 10% FBS. G401 cells were not transfected, and cell lysates and cell media were independently isolated and utilized for IP, as described above, but IP was performed using an anti-CRYAB mAb (Cell Signaling Technology, 45844). For this IP, the reaction tubes were +/− G401 conditioned media as this is the primary location of the majority of WT MYOC.

Isolation of cytoplasmic-only proteins

NTM5 cells were transfected with a control vector (pCMV-Tag1) or a CMV–MYOC Y437H plasmid. 48 h post-transfec-

tion, plates of cells were washed three times with 1× PBS. To each plate, 125 μl of Hypotonic lysis buffer (Sigma, ER0100) containing Roche Applied Science Complete protease inhibitors and 1 mM DTT was added for a 10-min incubation on ice. Cells were scraped from the plates and transferred into tubes that were then frozen on dry ice. Tubes were thawed, and following hard vortexing, the tubes were centrifuged at 7500 rpm at 4 °C for 5 min. The supernatant was transferred to a new tube, and the Bio-Rad DC protein assay completed. Samples were analyzed by Western blotting.

Thioflavin T staining

NTM5 cells were plated in Lab-Tek II chamber slides (Lab-Tek, 154461) and 24 h later transfected using FuGENE 6 (Promega, E2691) transfection reagent and maxi prep plasmids. 72 h post-transfection, cells were fixed using 4% paraformaldehyde solution. A 1% ThT solution (Sigma, T3516) was added to chamber slides for a 45-min incubation at room temperature. Following 1× PBS washes, a DAPI solution (Molecular Probes, D1306) was applied for 30 min. After additional 1× PBS washes, a coverslip was applied using VectaShield Hardmount (Vector Labs, H-1400). Slides were imaged using a Nikon BX-21 fluorescent microscope fitted with a ×40 objective.

Note that a limitation to ThT staining is that it cannot differentiate oligomeric intermediates (89). Additionally, disease severity does not necessarily correlate with the amount of amyloid deposition as small oligomers are also predicted to be highly toxic to cells (90). As ThT staining depends on the surface charge of the fiber (60), the staining intensity is influenced by exposed surface areas. Thus, a limitation to ThT staining is that it will predominantly stain aggregated proteins in which the protein precipitated state is highly ordered, and ThT may not be capable of staining aggregates formed by the amorphous aggregation pathway (91). Despite these drawbacks to the staining method, ThT does show excellent linearity between fibril concentration and ThT emission intensity (91). Amyloid staining is best viewed using transmission EM (91), but other microscopy methods can be utilized (83). Benefits of ThT staining surpass its limitations making ThT the "gold standard" for identifying amyloid fibrils (91).

Author contributions—J. M. L., B. Li, N. R., Y. K. W., T. B. N., E. M., D. R., and G. P. conceptualization; J. M. L., B. Leehy, and V. S.-V. data curation; J. M. L., B. Li, P. K., C. X., B. Leehy, V. S.-V., Y. K. W., E. M., D. R., G. P., and A. C. formal analysis; J. M. L., B. Li, N. R., Y. K. W., D. R., G. P., and A. C. supervision; J. M. L., B. Li, and P. K. validation; J. M. L., B. Li, P. K., C. X., B. Leehy, N. R., and V. S.-V. investigation; J. M. L., B. Li, P. K., C. X., B. Leehy, N. R., V. S.-V., H. L., T. B. N., D. R., and G. P. methodology; J. M. L. writing-original draft; J. M. L., Y. K. W., E. M., D. R., G. P., and A. C. project administration; J. M. L., B. Li, P. K., C. X., B. Leehy, N. R., V. S.-V., Y. K. W., H. L., T. B. N., E. M., D. R., G. P., and A. C. writing-review and editing; H. L., T. B. N., D. R., and G. P. resources.

References

1. Quigley, H. A., and Broman, A. T. (2006) The number of people with glaucoma worldwide in 2010 and 2020. *Br. J. Ophthalmol.* **90,** 262–267 CrossRef Medline
2. Friedman, D. S., Wolfs, R. C., O'Colmain, B. J., Klein, B. E., Taylor, H. R., West, S., Leske, M. C., Mitchell, P., Congdon, N., Kempen, J., and Eye Diseases Prevalence Research Group. (2004) Eye diseases prevalence research group. Prevalence of open-angle glaucoma among adults in the United States. *Arch. Ophthalmol.* **122,** 532–538 CrossRef Medline
3. Weinreb, R. N., Aung, T., and Medeiros, F. A. (2014) The pathophysiology and treatment of glaucoma. *JAMA* **311,** 1901–1911 CrossRef Medline
4. Meyer, A., Béchetoille, A., Valtot, F., Dupont de Dinechin, S., Adam, M. F., Belmouden, A., Brézin, A. P., Gomez, L., Bach, J. F., and Garchon, H. J. (1996) Age-dependent penetrance and mapping of the locus for juvenile and early-onset open-angle glaucoma on chromosome 1q (GLC1A) in a French family. *Hum. Genet.* **98,** 567–571 CrossRef Medline
5. Sunden, S. L., Alward, W. L., Nichols, B. E., Rokhlina, T. R., Nystuen, A., Stone, E. M., and Sheffield, V. C. (1996) Fine mapping of the autosomal dominant juvenile open angle glaucoma (GLC1A) region and evaluation of candidate genes. *Genome Res.* **6,** 862–869 CrossRef Medline
6. Stone, E. M., Fingert, J. H., Alward, W. L., Nguyen, T. D., Polansky, J. R., Sunden, S. L., Nishimura, D., Clark, A. F., Nystuen, A., Nichols, B. E., Mackey, D. A., Ritch, R., Kalenak, J. W., Craven, E. R., and Sheffield, V. C. (1997) Identification of a gene that causes primary open angle glaucoma. *Science* **275,** 668–670 CrossRef Medline
7. Tamm, E. R. (2002) Myocilin and glaucoma: facts and ideas. *Prog. Retin. Eye Res.* **21,** 395–428 CrossRef Medline
8. Fingert, J. H., Héon, E., Liebmann, J. M., Yamamoto, T., Craig, J. E., Rait, J., Kawase, K., Hoh, S. T., Buys, Y. M., Dickinson, J., Hockey, R. R., Williams-Lyn, D., Trope, G., Kitazawa, Y., Ritch, R., Mackey, D. A., Alward, W. L., Sheffield, V. C., and Stone, E. M. (1999) Analysis of myocilin mutations in 1703 glaucoma patients from five different populations. *Hum. Mol. Genet.* **8,** 899–905 CrossRef Medline
9. Johnson, D. (2000) Myocilin and glaucoma: a TIGR by the tail? *Arch. Ophthalmol.* **118,** 974–978 Medline
10. Shimizu, S., Lichter, P. R., Johnson, A. T., Zhou, Z., Higashi, M., Gottfredsdottir, M., Othman, M., Moroi, S. E., Rozsa, F. W., Schertzer, R. M., Clarke, M. S., Schwartz, A. L., Downs, C. A., Vollrath, D., and Richards, J. E. (2000) Age-dependent prevalence of mutations at the GLC1A locus in primary open-angle glaucoma. *Am. J. Ophthalmol.* **130,** 165–177 CrossRef Medline
11. Morissette, J., Clépet, C., Moisan, S., Dubois, S., Winstall, E., Vermeeren, D., Nguyen, T. D., Polansky, J. R., Côté, G., Anctil, J. L., Amyot, M., Plante, M., Falardeau, P., and Raymond, V. (1998) Homozygotes carrying an autosomal dominant TIGR mutation do not manifest glaucoma. *Nat. Genet.* **19,** 319–321 CrossRef Medline
12. Alward, W. L. (2000) The genetics of open-angle glaucoma: the story of GLC1A and myocilin. *Eye* **14,** 429–436 CrossRef Medline
13. Gobeil, S., Letartre, L., and Raymond, V. (2006) Functional analysis of the glaucoma-causing TIGR/myocilin protein: integrity of amino-terminal coiled-coil regions and olfactomedin homology domain is essential for extracellular adhesion and secretion. *Exp. Eye Res.* **82,** 1017–1029 CrossRef Medline
14. Jacobson, N., Andrews, M., Shepard, A. R., Nishimura, D., Searby, C., Fingert, J. H., Hageman, G., Mullins, R., Davidson, B. L., Kwon, Y. H., Alward, W. L., Stone, E. M., Clark, A. F., and Sheffield, V. C. (2001) Non-secretion of mutant proteins of the glaucoma gene myocilin in cultured trabecular meshwork cells and in aqueous humor. *Hum. Mol. Genet.* **10,** 117–125 CrossRef Medline
15. Souzeau, E., Burdon, K. P., Dubowsky, A., Grist, S., Usher, B., Fitzgerald, J. T., Crawford, A., Hewitt, A. W., Goldberg, I., Mills, R. A., Ruddle, J. B., Landers, J., Mackey, D. A., and Craig, J. E. (2013) Higher prevalence of myocilin mutations in advanced glaucoma in comparison with less advanced disease in an Australian disease registry. *Ophthalmology* **120,** 1135–1143 CrossRef Medline
16. Alward, W. L., Fingert, J. H., Coote, M. A., Johnson, A. T., Lerner, S. F., Junqua, D., Durcan, F. J., McCartney, P. J., Mackey, M. B., Sheffield, V. C., and Stone, E. M. (1998) Clinical features associated with mutations in the chromosome open-angle glaucoma gene (GLC1A). *N. Eng. J. Med.* **338,** 1022–1027 CrossRef
17. Zhuo, Y. H., Wei, Y. T., Bai, Y. J., Duan, S., Lin, M. K., Saragovi, H. U., and Ge, J. (2008) Pro370Leu *MYOC* gene mutation in a large Chinese family

with juvenile-onset open angle glaucoma: correlation between genotype and phenotype. *Mol. Vis.* **14,** 1533–1539 Medline

18. Li, C. M., Zhang, Y. H., Ye, R. H., Yi, C. X., Zhong, Y. M., Cao, D., and Liu, X. (2014) Anticipation, anti-glaucoma drug treatment response and phenotype of a Chinese family with glaucoma caused by the Pro370Leu myocilin mutation. *Int. J. Ophthalmol.* **7,** 44–50 Medline
19. Kwon, Y. H., Fingert, J. H., Kuehn, M. H., and Alward, W. L. (2009) Primary open-angle glaucoma. *N. Engl. J. Med.* **360,** 1113–1124 CrossRef Medline
20. Nag, A., Lu, H., Arno, M., Iglesias, A. I., Bonnemaijer, P., Broer, L., Uitterlinden, A. G., Klaver, C. C., van Duijn, C., Hysi, P. G., and Hammond, C. J. (2017) Evaluation of the myocilin mutation Gln368Stop demonstrates reduced penetrance for glaucoma in European populations. *Ophthalmology* **124,** 547–553 CrossRef Medline
21. Adam, M. F., Belmouden, A., Binisti, P., Brézin, A. P., Valtot, F., Béchetoille, A., Dascotte, J. C., Copin, B., Gomez, L., Chaventré, A., Bach, J. F., and Garchon, H. J. (1997) Recurrent mutations in a single copy exon encoding the evolutionarily conserved olfactomedin-homology domain of TIGR in familial open-angle glaucoma. *Hum. Mol. Genet.* **6,** 2091–2097 CrossRef Medline
22. Nguyen, T. D., Chen, P., Huang, W. D., Chen, H., Johnson, D., and Polansky, J. R. (1998) Gene structure and properties of TIGR, an olfactomedin-related glycoprotein cloned from glucocorticoid-induced trabecular meshwork cells. *J. Biol. Chem.* **273,** 6341–6350 CrossRef Medline
23. Ortego, J., Escribano, J., and Coca-Prados, M. (1997) Cloning and characterization of subtracted cDNAs from a human ciliary body library encoding TIGR, a protein involved in juvenile open angle glaucoma with homology to myosin and olfactomedin. *FEBS Lett.* **413,** 349–353 CrossRef Medline
24. Kim, B. S., Savinova, O. V., Reedy, M. V., Martin, J., Lun, Y., Gan, L., Smith, R. S., Tomarev, S. I., John, S. W., and Johnson, R. L. (2001) Targeted disruption of the myocilin gene (Myoc) suggests that human glaucoma-causing mutations are gain of function. *Mol. Cell. Biol.* **21,** 7707–7713 CrossRef Medline
25. Senatorov, V., Malyukova, I., Fariss, R., Wawrousek, E. F., Swaminathan, S., Sharan, S. K., and Tomarev, S. (2006) Expression of mutated mouse myocilin induces open-angle glaucoma in transgenic mice. *J. Neurosci.* **26,** 11903–11914 CrossRef Medline
26. Zhou, Y., Grinchuk, O., and Tomarev, S. I. (2008) Transgenic mice expressing the Tyr437His mutant of human myocilin protein develop glaucoma. *Invest. Ophthalmol. Vis. Sci.* **49,** 1932–1939 CrossRef Medline
27. Zillig, M., Wurm, A., Grehn, F. J., Russell, P., and Tamm, E. R. (2005) Overexpression and properties of wild-type and Tyr437His mutated myocilin in the eyes of transgenic mice. *Invest. Ophthalmol. Vis. Sci.* **46,** 223–234 CrossRef Medline
28. Shepard, A. R., Jacobson, N., Millar, J. C., Pang, I. H., Steely, H. T., Searby, C. C., Sheffield, V. C., Stone, E. M., and Clark, A. F. (2007) Glaucoma-causing myocilin mutants require the peroxisomal targeting signal-1 receptor (PTS1R) to elevate intraocular pressure. *Hum. Mol. Gen.* **16,** 609–617 CrossRef Medline
29. Elgersma, Y., Vos, A., van den Berg, M., van Roermund, C. W., van der Sluijs, P., Distel, B., and Tabak, H. F. (1996) Analysis of the carboxyl-terminal peroxisomal targeting signal 1 in a homologous context in *Saccharomyces cerevisiae*. *J. Biol. Chem.* **271,** 26375–26382 CrossRef Medline
30. Brocard, C., and Hartig, A. (2006) Peroxisome targeting signal 1: is it really a simple tripeptide? *Biochim. Biophys. Acta* **1763,** 1565–1573 CrossRef Medline
31. Swinkels, B. W., Gould, S. J., and Subramani, S. (1992) Targeting efficiencies of various permutations of the consensus C-terminal tripeptide peroxisomal targeting signal. *FEBS Lett.* **305,** 133–136 CrossRef Medline
32. Lametschwandtner, G., Brocard, C., Fransen, M., Van Veldhoven, P., Berger, J., and Hartig, A. (1998) The difference in recognition of terminal tripeptides as peroxisomal targeting signal 1 between yeast and human is due to different affinities of their receptor Pex5p to the cognate signal and to residues adjacent to it. *J. Biol. Chem.* **273,** 33635–33643 CrossRef Medline
33. Donegan, R. K., Hill, S. E., Freeman, D. M., Nguyen, E., Orwig, S. D., Turnage, K. C., and Lieberman, R. L. (2015) Structural basis for misfolding in myocilin-associated glaucoma. *Hum. Mol. Genet.* **24,** 2111–2124 CrossRef Medline
34. Zode, G. S., Kuehn, M. H., Nishimura, D. Y., Searby, C. C., Mohan, K., Grozdanic, S. D., Bugge, K., Anderson, M. G., Clark, A. F., Stone, E. M., and Sheffield, V. C. (2011) Reduction of ER stress via a chemical chaperone prevents disease phenotypes in a mouse model of primary open angle glaucoma. *J. Clin. Invest.* **121,** 3542–3553 CrossRef Medline
35. Wiggs, J. L., Allingham, R. R., Vollrath, D., Jones, K. H., De La Paz, M., Kern, J., Patterson, K., Babb, V. L., Del Bono, E. A., Broomer, B. W., Pericak-Vance, M. A., and Haines, J. L. (1998) Prevalence of mutations in TIGR/myocilin in patients with adult and juvenile primary open-angle glaucoma. *Am. J. Hum. Genet.* **63,** 1549–1552 CrossRef Medline
36. Shepard, A. R., Jacobson, N., Sui, R., Steely, H. T., Lotery, A. J., Stone, E. M., and Clark, A. F. (2003) Characterization of rabbit myocilin: implications for human myocilin glycosylation and signal peptide usage. *BMC Genet.* **4,** 5 CrossRef Medline
37. Polansky, J. R., Fauss, D. J., and Zimmerman, C. C. (2000) Regulation of TIGR/MYOC gene expression in human trabecular meshwork cells. *Eye* **14,** 503–514 CrossRef Medline
38. Ishibashi, T., Takagi, Y., Mori, K., Naruse, S., Nishino, H., Yue, B. Y., and Kinoshita, S. (2002) cDNA microarray analysis of gene expression changes induced by dexamethasone in cultured human trabecular meshwork cells. *Invest. Ophthalmol. Vis. Sci.* **43,** 3691–3697 Medline
39. Miyara, N., Shinzato, M., Yamashiro, Y., Iwamatsu, A., Kariya, K. L., and Sawaguchi, S. (2008) Protomic analysis of rat retina in a steroid-induced ocular hypertenision model: potential vulnerability to oxidative stress. *Jpn. J. Ophthalmol.* **52,** 84–90 CrossRef Medline
40. Bui, B. V., and Fortune, B. (2004) Ganglion cell contributions to the rat full-field electroretinogram. *J. Physiol.* **555,** 153–173 CrossRef Medline
41. Penn, R. D., and Hagins, W. A. (1969) Signal transmission along retinal rods and the origin of the electroretinographic a-wave. *Nature* **223,** 201–204 CrossRef Medline
42. Chou, T. H., Tomarev, S., and Porciatti, V. (2014) Transgenic mice expressing mutated Tyr437His human myocilin develop progressive loss of retinal ganglion cell electrical responsiveness and axonopathy with normal IOP. *Invest. Ophthalmol. Vis. Sci.* **55,** 5602–5609 CrossRef Medline
43. Aroca-Aguilar, J. D., Sanchez-Sanchez, F., Ghosh, S., Navarro, A. F., Coca-Prados, M., and Escribano, J. (2011) Interaction of recombinant myocilin with the matricellular protein SPARC: functional implications. *Invest. Ophthalmol. Vis. Sci.* **52,** 179–189 CrossRef
44. Fautsch, M. P., Vrabel, A. M., and Johnson, D. H. (2006) The identification of myocilin-associated proteins in the human trabecular meshwork. *Exp. Eye Res.* **82,** 1046–1052 CrossRef Medline
45. Wentz-Hunter, K., Ueda, J., and Yue, B. Y. (2002) Protein interactions with myocilin. *Invest. Ophthalmol. Vis. Sci.* **43,** 176–182 Medline
46. Anholt, R. R., and Carbone, M. A. (2013) A molecular mechanism for glaucoma: endoplasmic reticulum stress and the unfolded protein response. *Trends Mol. Med.* **19,** 586–593 CrossRef Medline
47. Caballero, M., and Borrás, T. (2001) Inefficient processing of an olfactomedin-deficient myocilin mutant: potential physiological relevance to glaucoma. *Biochem. Biophys. Res. Commun.* **282,** 662–670 CrossRef Medline
48. Yam, G. H., Gaplovska-Kysela, K., Zuber, C., and Roth, J. (2007) Sodium 4-phenylbutyrate acts as a chemical chaperone on misfolded myocilin to rescue cells from endoplasmic reticulum stress and apoptosis. *Invest. Ophthalmol. Vis. Sci.* **48,** 1683–1690 CrossRef Medline
49. Gould, D. B., Reedy, M., Wilson, L. A., Smith, R. S., Johnson, R. L., and John, S. W. (2006) Mutant myocilin nonsecretion *in vivo* is not sufficient to cause glaucoma. *Mol. Cell. Biol.* **26,** 8427–8436 CrossRef Medline
50. Lütjen-Drecoll, E., May, C. A., Polansky, J. R., Johnson, D. H., Bloemendal, H., and Nguyen, T. D. (1998) Localization of the stress proteins αB-crystallin and trabecular meshwork inducible glucocorticoid response protein in normal and glaucomatous trabecular meshwork. *Invest. Ophthalmol. Vis. Sci.* **39,** 517–525 Medline
51. Kore, R. A., and Abraham, E. C. (2016) Phosphorylation negatively regulates exosome mediated secretion of CRYAB in glioma cells. *Biochim. Biophys. Acta* **1863,** 368–377 CrossRef Medline

52. Snider, E. J., Vannatta, R. T., Schildmeyer, L., Stamer, W. D., and Ethier, C. R. (2018) Characterizing differences between MSCs and TM cells: towards autologous stem cell therapies for the glaucomatous trabecular meshwork. *J. Tissue Eng. Regen. Med.* **12,** 695–704 CrossRef Medline
53. Brubaker, R. F. (1998) in *Eye's Aqueous Humor: From Secretion to Glaucoma* (Civan, M. M., ed) pp. 234–284, Academic Press, San Diego
54. Johnson, M., McLaren, J. W., and Overby, D. R. (2017) Unconventional aqueous humor outflow: a review. *Exp Eye. Res.* **158,** 94–111 CrossRef Medline
55. Andley, U. P. (2007) Crystallins in the eye: function and pathology. *Prog. Retin. Eye Res.* **26,** 78–98 CrossRef Medline
56. Piri, N., Song, M., Kwong, J. M., and Caprioli, J. (2007) Modulation of α and β crystallin expression in retinas with ocular hypertension-induced ganglion cell degeneration. *Brain Res.* **1141,** 1–9 CrossRef Medline
57. Steele, M. R., Inman, D. M., Calkins, D. J., Horner, P. J., and Vetter, M. L. (2006) Microarray analysis of retinal gene expression in th eDBA/2J model of glaucoma. *Invest. Ophthalmol. Vis. Sci.* **47,** 977–985 CrossRef Medline
58. Mirzaei, M., Gupta, V. B., Chick, J. M., Greco, T. M., Wu, Y., Chitranshi, N., Wall, R. V., Hone, E., Deng, L., Dheer, Y., Abbasi, M., Rezaeian, M., Braidy, N., You, Y., Salekdeh, G. H., *et al.* (2017) Age-related neurodegenerative disease associated pathways identified in retinal and vitreous proteome from human glaucoma eyes. *Sci. Rep.* **7,** 12685 CrossRef Medline
59. Benjamin, I. J., and McMillan, D. R. (1998) Stress (heat shock) proteins: molecular chaperones in cardiovascular biology and disease. *Circ. Res.* **83,** 117–132 CrossRef Medline
60. Ecroyd, H., Meehan, S., and Carver, J. A. (2010) in *Small Stress Proteins and Human Diseases* (Simon, S., and Arrigo, A. P., eds) pp. 189–211, Nova Science Publishers, New York
61. Hagemann, T. L., Boelens, W. C., Wawrousek, E. F., and Messing, A. (2009) Suppression of GFAP toxicity by $\alpha\beta$-crystallin in mouse models of Alexander disease. *Hum. Mol. Genet.* **18,** 1190–1199 CrossRef Medline
62. Oliveira, A. O., Osmand, A., Outeiro, T. F., Muchowski, P. J., and Finkbeiner, S. (2016) $\alpha\beta$-Crystallin overexpression in astrocytes modulates the phenotype of the BACHD mouse model of Huntington's disease. *Hum. Mol. Genet.* **25,** 1677–1689 CrossRef Medline
63. Hamanaka, T., Kimura, M., Sakurai, T., Ishida, N., Yasuda, J., Nagasaki, M., Nariai, N., Endo, A., Homma, K., Katsuoka, F., Matsubara, Y., Yamamoto, M., and Fuse, N. (2017) A histologic categorization of aqueous outflow routes in familial open-angle glaucoma and associations with mutations in the MYOC gene in Japanese patients. *Invest. Ophthalmol. Vis. Sci.* **58,** 2818–2831 CrossRef Medline
64. Glembotski, C. (2007) Endoplasmic reticulum stress in the heart. *Circ. Res.* **101,** 975–984 CrossRef Medline
65. Qiu, Y., Shen, X., Shyam, R., Yue, B. Y., and Ying, H. (2014) Cellular processing of myocilin. *PLoS One* **9,** e92845 CrossRef Medline
66. Lynch, J. M., Maillet, M., Vanhoutte, D., Schloemer, A., Sargent, M. A., Blair, N. S., Lynch, K. A., Okada, T., Aronow, B. J., Osinska, H., Prywes, R., Lorenz, J. N., Mori, K., Lawler, J., Robbins, J., and Molkentin, J. D. (2012) A thrombospondin-dependent pathway for a protective ER stress response. *Cell* **149,** 1257–1268 CrossRef Medline
67. Joe, M. K., Sohn, S., Hur, W., Moon, Y., Choi, Y. R., and Kee, C. (2003) Accumulation of mutant myocilins in ER leads to ER stress and potential cytotoxicity in human trabecular meshwork cells. *Biochem. Biophys. Res. Commun.* **312,** 592–600 CrossRef Medline
68. Eisele, Y. S., Monteiro, C., Fearns, C., Encalada, S. E., Wiseman, R. L., Powers, E. T., and Kelly, J. W. (2015) Targeting protein aggregation for the treatment of degenerative diseases. *Nat. Rev. Drug Discov.* **14,** 759–780 CrossRef Medline
69. Hill, S. E., Donegan, R. K., Nguyen, E., Desai, T. M., and Lieberman, R. L. (2015) Molecular details of olfactomedin domains provide pathway to structure-function studies. *PLoS One* **10,** e0130888 CrossRef Medline
70. Arrigo, A. P., Simon, S., Gibert, B., Kretz-Remy, C., Nivon, M., Czekalla, A., Guillet, D., Moulin, M., Diaz-Latoud, C., and Vicart, P. (2007) Hsp27 (HspB1) and αB-crystallin (HspB5) as therapeutic targets. *FEBS Lett.* **581,** 3665–3674 CrossRef Medline
71. Scheier, B., Foletti, A., Stark, G., Aoyama, A., Döbbeling, U., Rusconi, S., and Klemenz, R. (1996) Glucocorticoids regulate the expression of the stress protein αB-crystallin. *Mol. Cell. Endocrinol.* **123,** 187–198 CrossRef Medline
72. Schlunck, G., Han, H., Wecker, T., Kampik, D., Meyer-ter-Vehn, T., and Grehn, F. (2008) Substrate rigidity modulates cell-matrix interactions and protein expression in human trabecular meshwork cells. *Invest. Ophthalmol. Vis. Sci.* **49,** 262–269 Medline
73. Jobling, A. I., Stevens, A., and Augusteyn, R. C. (2001) Binding of dexamethasone by α-crystallin. *Invest. Ophthalmol. Vis. Sci.* **42,** 1829–1832 Medline
74. Johnson, W. G. (1980) A metabolic interference and the +/− heterozygote. A hypothetical form of simple inheritance which is neither dominant nor recessive. *Am. J. Hum. Genet.* **32,** 374–386 Medline
75. Wirtz, M. K., Konstas, A. G., Samples, J. R., Kaltsos, K., Economou, A., Dimopoulos, A., Georgiadou, I., and Petersen, M. B. (2008) Myocilin variations and familial glaucoma in Taxiarchis, a small Greek village. *Mol. Vis.* **14,** 774–781 Medline
76. Faucher, M., Anctil, J. L., Rodrigue, M. A., Duchesne, A., Bergeron, D., Blondeau, P., Côté, G., Dubois, S., Bergeron, J., Arseneault, R., Morissette, J., Raymond, V., and Québec Glaucoma Network. (2002) Founder TIGR/myocilin mutations for glaucoma in the Quebec population. *Hum. Mol. Genet.* **11,** 2077–2090 CrossRef Medline
77. Young, T. K., Souzeau, E., Liu, L., Kearns, L. S., Burdon, K. P., Craig, J. E., and Ruddle, J. B. (2012) Compound heterozygote myocilin mutations in a pedigree with high prevalence of primary open-angle glaucoma. *Mol. Vis.* **18,** 3064–3069 DOI not found. Medline
78. Röcken, C., Linke, R. P., and Saeger, W. (1992) Immunohistology of islet amyloid polypeptide in diabetes mellitus: semi-quantitative studies in a post-mortem series. *Virchows Arch. A Pathol. Anat. Histopathol.* **421,** 339–344 CrossRef Medline
79. Jones-Odeh, E., and Hammond, C. J. (2015) How strong is the relationship between glaucoma, the retinal nerve fibre layer, and neurodegenerative disease such as Alzheimer's disease and multiple sclerosis? *Eye* **29,** 1270–1284 CrossRef Medline
80. Stothert, A. R., Suntharalingam, A., Huard, D. J., Fontaine, S. N., Crowley, V. M., Mishra, S., Blagg, B. S., Lieberman, R. L., and Dickey, C. A. (2014) Exploiting the interaction between Grp94 and aggregated myocilin to treat glaucoma. *Hum. Mol. Genet.* **23,** 6470–6480 CrossRef Medline
81. Chis, R., Sharma, P., Bousette, N., Miyake, T., Wilson, A., Backx, P. H., and Gramolini, A. O. (2012) α-Crystallin B prevents apoptosis after H_2O_2 exposure in mouse neonatal cardiomyocytes. *Am. J. Physiol. Heart Circ. Physiol.* **303,** H967–H978 CrossRef Medline
82. Piri, N., Kwong, J. M., and Caprioli, J. (2013) Crystallins in retinal ganglion cell survival and regeneration. *Mol. Neurobiol.* **48,** 819–828 CrossRef Medline
83. Massaad, C. A., Washington, T. M., Pautler, R. G., and Klann, E. (2009) Overexpression of SOD-2 reduces hippocampal superoxide and prevents memory deficits in a mouse model of Alzheimer's disease. *Proc. Natl. Acad. Sci. U.S.A.* **106,** 13576–13581 CrossRef Medline
84. Makley, L. N., McMenimen, K. A., DeVree, B. T., Goldman, J. W., McGlasson, B. N., Rajagopal, P., Dunyak, B. M., McQuade, T. J., Thompson, A. D., Sunahara, R., Klevit, R. E., Andley, U. P., and Gestwicki, J. E. (2015) Pharmacological chaperone for α-crystallin partially restores transparency in cataract models. *Science* **350,** 674–677 CrossRef Medline
85. Lundvall, A., Svedberg, H., and Chen, E. (2011) Application of the ICare rebound tonometer in healthy infants. *J. Glaucoma* **20,** 7–9 CrossRef Medline
86. Pang, I. H., Shade, D. L., Clark, A. F., Steely, H. T., and DeSantis, L. (1994) Preliminary characterization of a transformed cell strain derived from human trabecular meshwork. *Curr. Eye Res.* **13,** 51–63 CrossRef Medline
87. Liton, P. B., Luna, C., Challa, P., Epstein, D. L., and Gonzalez, P. (2006) Genome-wide expression profile of human trabecular meshwork cultured cells, nonglaucomatous and primary open angle glaucoma tissue. *Mol. Vis.* **12,** 774–790 Medline
88. Shevchenko, A., Tomas, H., Havlis, J., Olsen, J. V., and Mann, M. (2006) In-gel digestion for mass spectrometric characterization of proteins and proteomes. *Nat. Protoc.* **1,** 2856–2860 Medline
89. Maezawa, I., Hong, H. S., Liu, R., Wu, C. Y., Cheng, R. H., Kung, M. P., Kung, H. F., Lam, K. S., Oddo, S., Laferla, F. M., and Jin, L. W. (2008) Congo

red and thioflavin-T analogs detect Aβ oligomers. *J. Neurochem.* **104,** 457–468 Medline

90. Patel, H. R., Pithadia, A. S., Brender, J. R., Fierke, C. A., and Ramamoorthy, A. (2014) In search of aggregation pathways of IAPP and other amyloidogenic proteins: finding answers through NMR spectroscopy. *J. Phys. Chem. Lett.* **5,** 1864–1870 CrossRef Medline
91. Gade Malmos, K., Blancas-Mejia, L. M., Weber, B., Buchner, J., Ramirez-Alvarado, M., Naiki, H., and Otzen, D. (2017) TnT 101: a primer on the use of thioflavin T to investigate amyloid formation. *Amyloid* **24,** 1–16 CrossRef Medline
92. Hewitt, A. W., Mackey, D. A., and Craig, J. E. (2008) Myocilin allele-specific glaucoma phenotype database. Hum. Mutat. 29, 207–211 CrossRef Medline